Xie *et al. Energy Mater* 2024;4:400007
DOI: 10.20517/energymater.2023.70

Energy Materials

Review

Open Access

Review on Fe-based double perovskite cathode materials for solid oxide fuel cells

Manyi Xie[1,2,#], Changkun Cai[1,2,#], Xingyu Duan[4], Ke Xue[1,2], Hong Yang[3,*], Shengli An[1,2,*]

[1]Inner Mongolia Key Laboratory of Advanced Ceramic Materials and Devices, School of Materials and Metallurgy, Inner Mongolia University of Science and Technology, Baotou 014010, Inner Mongolia, China.
[2]Key Laboratory of Green Extraction & Efficient Utilization of Light Rare-Earth Resources (Inner Mongolia University of Science and Technology), Ministry of Education, Baotou 014010, Inner Mongolia, China.
[3]School of Engineering, The University of Western Australia, Perth, WA 6009, Australia.
[4]Guizhou High Level Institution Key Laboratory of High-Performance Battery Materials, Guizhou University, Guiyang 550025, Guizhou, China.
[#]Authors contributed equally.

***Correspondence to:** Prof. Shengli An, Key Laboratory of Green Extraction & Efficient Utilization of Light Rare-Earth Resources, (Inner Mongolia University of Science and Technology), Ministry of Education, Arding Street No. 7, Baotou 014010, Inner Mongolia, China. E-mail: san@imust.edu.cn; Prof. Hong Yang, School of Engineering, The University of Western Australia, 35 Stirling Highway Perth, WA 6009, Australia. E-mail: hong.yang@uwa.edu.au

How to cite this article: Xie M, Cai C, Duan X, Xue K, Yang H, An S. Review on Fe-based double perovskite cathode materials for solid oxide fuel cells. *Energy Mater* 2024;4:400007. https://dx.doi.org/10.20517/energymater.2023.70

Received: 2 Sep 2023 **First Decision:** 11 Oct 2023 **Revised:** 31 Oct 2023 **Accepted:** 22 Nov 2023 **Published:** 8 Jan 2024

Academic Editor: Bin Zhu **Copy Editor:** Fangyuan Liu **Production Editor:** Fangyuan Liu

Abstract

As a clean and efficient energy conversion device, solid oxide fuel cells have been garnering attention due to their environmentally friendly and fuel adaptability. Consequently, they have become one of the current research directions of new energy. The cathode, as the electrochemical reaction site of an oxidation atmosphere in solid oxide fuel cells, plays a key role in determining the output performance. In recent years, the development of double perovskite cathode materials with mixed ionic and electronic conductors has made significant progress in intermediate-temperature (600-800 °C) fuel cells. These materials have the potential to deliver higher power densities and improved stability, making them promising candidates for future fuel cell applications. The Fe-based double perovskite structure cathode material has gained extensive attention due to its adjustable crystal structure and performance, as it has A(A′) or B(B′) positions in its $AA'BB'O_6$ structure. This material has several advantages, such as high oxygen catalytic activity, low thermal expansion coefficient, and compatibility with the thermal expansion of the electrolyte. An increasing number of researchers have been exploring the performance reaction mechanism of double perovskite by modifying and adjusting its material microstructure, crystal structure, and electronic structure. In this paper, the research progress of $LnBaFe_2O_5$ and $Sr_2Fe_{2-x}Mo_xO_6$ double perovskite cathode

materials is reviewed to highlight the effects of various modification methods developed on electrochemical performance of these materials. Furthermore, the potential future research directions of double perovskite cathode materials are prospected.

Keywords: Solid oxide fuel cell, double perovskite oxide, Sr_2FeMoO_6, $LnBaFe_2O_5$, electrochemical performance

INTRODUCTION

Energy is not only essential in driving a country's economic development around the world but is also becoming an increasingly important indicator of the overall strength and level of civilization of the nation and the living standard of its people. Today, the energy decision-making and the technological orientation of a country are also rightfully influenced by the need for environmental protection and green development, which together form the cornerstones of a sustainable development strategy. The development of efficient, safe, and low-cost new clean energy is an inevitable trend of future economic development of any human society[1]. Among the many clean energy systems, the solid oxide fuel cell (SOFC) technology has been favored due to its environmental friendliness, high efficiency, and great potential for use in large-scale energy generation and distribution and in combined heat and power generation[2,3]. At present, the SOFC technology is being actively developed as the energy supply in ships, aerospace, vehicles, and other applications[4]. Figure 1 depicts the application fields of SOFCs and the demanded power capacity.

Figure 2 depicts the configuration and working principle of a SOFC stack. As seen, a single SOFC is composed of three main functional components: a cathode, an anode, and an electrolyte. Essentially, on the cathode surface, oxygen (O_2) is reduced to oxygen ions (O^{2-}) via the oxygen reduction reaction (ORR). O^{2-} ions are then transferred to the anode through the electrolyte. On the anode surface, hydrogen (H_2) is oxidized by O^{2-} form H_2O. This also releases electrons that pass through the external circuit and flow back to the cathode to form a closed circuit[5].

While significant progress has been made since its inception, the SOFC technology still faces some challenges, such as limited stability and high cost, both caused by the need for high operating temperatures (typically > 1,000 °C)[6-8]. To enable widespread applications, it is essential that the SOFC can operate effectively at the intermediate temperature (IT) range of 600-800 °C. Currently, this is largely hindered by the unsatisfactory performance of the cathode material due to serious polarization loss at reduced operating temperatures. Over the years, significant effort has been directed at the research and development (R&D) of cathode materials, which has resulted in a high volume of research output. The motivation of this review is to summarize the progress being made, highlight the remaining challenges, and hopefully identify the way forward for the near future R&D of cathode materials to support the IT-SOFC technology.

The development of the cathode material for SOFC started mostly with oxides loaded with precious metals for oxygen catalytic activity, such as Pd, Pt, or Au loaded on CeO_2[9] and other oxides[10,11]. It was quickly abandoned due to the high cost and limited reserves, which would prevent the intended large-scale commercialization of SOFC technology[9-11]. The attention was quickly shifted to perovskite oxides (see Note below), such as $La_{1-x}Sr_xMnO_3$, when it was discovered to have excellent oxygen catalytic activity at 800-1,000 °C[12]. However, as a pure electronic conductor, the ORR could only occur at the interface of the cathode and electrolyte[13]. This results in very limited catalytic efficiency of the cathode.

With this understanding comes the development of several mixed ionic and electronic conductors (MIEC) such as $La_{0.6}Sr_{0.4}Co_{0.2}Fe_{0.8}O_3$[14] and $SmBaFe_2O_5$ (SBF)[15]. Serving as a cathode in SOFC, the MIEC greatly

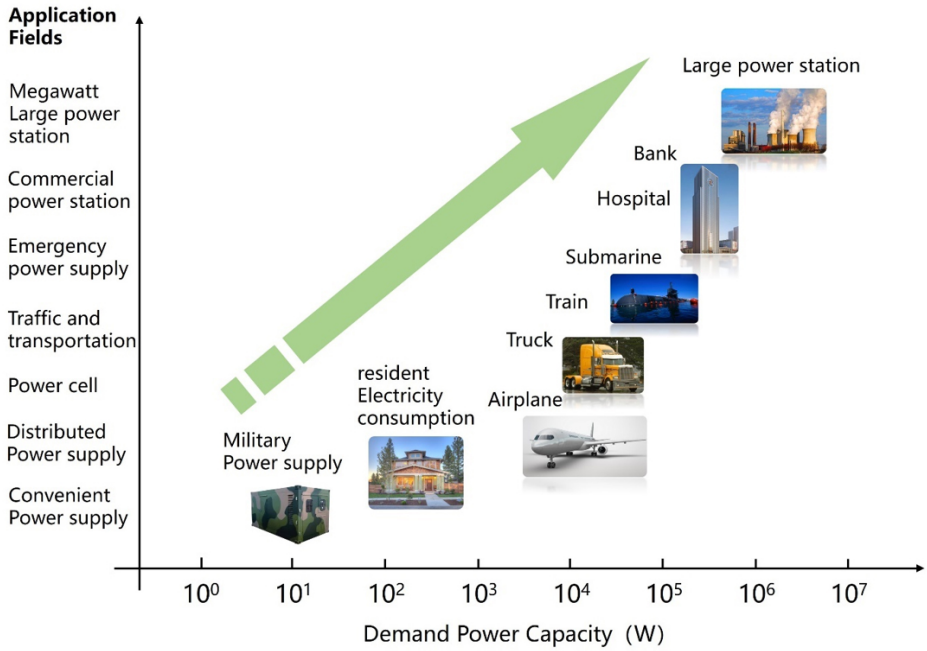

Figure 1. The application fields and the demanded power capacity of solid oxide fuel cells in the future.

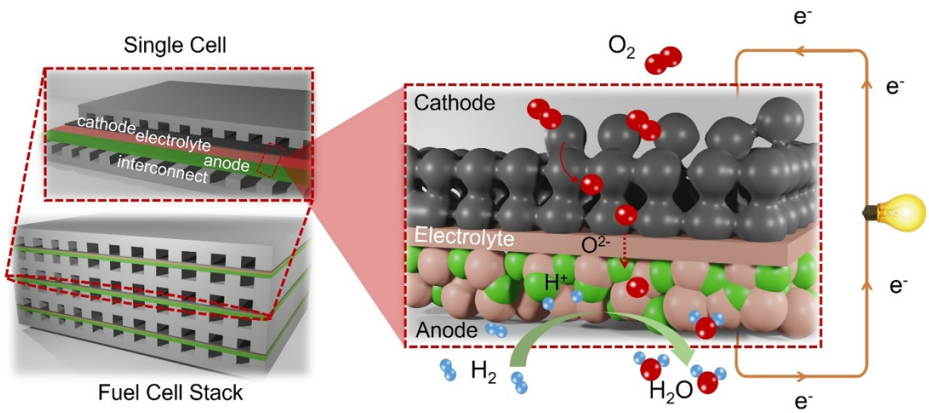

Figure 2. The configuration of a fuel cell stack and working principle of a solid oxide fuel cell.

enhances the ORR efficiency by extending the reaction sites from the limitation of a cathode-electrolyte interface to the entire cathode. Meanwhile, some of these conductors also display excellent electrochemical performance at the specified IT range[16-21]. Among the various MIEC cathode materials studied so far, double perovskite oxides have gained attention in recent years, particularly several Fe-based double perovskite oxides. It has been found that a double perovskite structure has a high capacity to accommodate non-stoichiometric oxygen, which would increase the concentration of oxygen vacancies, enhance the mobility of oxygen ions, and consequently facilitate the adsorption and dissociation of oxygen in the oxide[22,23]. The Fe-based double perovskites have additional advantages, including being cost-effective, having excellent structural stability, and having multiple sites for property modification[22-24]. However, they do suffer from intrinsically low oxygen transport kinetics due to the formation of Fe-O-Fe bonds. This is driving intensive research activities on a wide range of approaches aimed at enhancing ORR performance on Fe-based double perovskite cathode materials.

This review will focus on the current development of Fe-based double perovskite cathode materials, particularly the $Sr_2Fe_{2-x}Mo_xO_6$ and $LnBaFe_2O_5$ systems. As highlighted in Figure 3, it will provide an overview of the current achievements through element doping, electrode surface modification, and composite electrode formation on the cathode performance.

FE-BASED DOUBLE PEROVSKITE CATHODE MATERIALS

Types of perovskite oxide-based cathode materials

Figure 4 presents the structure characteristics of several types of perovskite oxides, including simple and double perovskite oxides.

Figure 4A presents the lattice structure of a simple perovskite oxide. Essentially, a simple perovskite oxide has a general formula of ABO_3, where an A-site is typically occupied by an alkali or lanthanide rare earth metal and a B-site is occupied by a transition metal. It has an idealized Pm-3m cubic crystal structure, in which BO_6 octahedrons share corners to form the lattice skeleton with A-sites located in the void centers within the skeleton[25].

A double perovskite oxide, as the name suggests, consists of two different perovskite structure units of ABO_3 and $A'B'O_3$. Depending on detailed occupancy of A and B sites, the oxide could be further divided into the B-site double perovskite (where A and A' are occupied by the same element, yet B and B' are not the same) or A-site double perovskite (where A and A' are not the same, but B and B' are the same).

Figure 4B illustrates a B-site $A_2BB'O_6$ double perovskite structure, where A-sites are mainly occupied by ions of alkali earth metals (such as Ba^{2+}, Sr^{2+}) or ions of rare earth elements with relatively large ionic radius (such as La^{3+}, Pr^{3+}, Nd^{3+}, Sm^{3+}, and Gd^{3+}). On the other hand, the B(B')-sites are typically occupied by ions of transition metals of relatively lower valence state (such as Fe^{3+}, Co^{3+}, and Ni^{2+}) and those of higher valence state (such as Mo^{6+}, W^{6+}, and Nb^{5+}). To balance the charge distribution and minimize the distortion to the lattice caused by the differences in valence state and size between the two B-site elements, they are typically arranged in an orderly manner within the structure. The oxygen octahedron formed by B and B' is arranged alternately along the three axes of a/b/c, and B and B' atoms are connected to form B-O-B' through oxygen atoms[26].

Figure 4C depicts an A-site $AA'B_2O_6$ double perovskite structure, where an oxygen octahedron composed of transition metal elements forms a lattice skeleton, and the A-site and A'-site elements are arranged alternatingly above and below the octahedron arrays. In the case where the radii of two elements on the A- and A'- sites are significantly different, $AA'B_2O_6$ adopts a layered structure, as depicted in Figure 4D. Here, the A- and A'- sites are arranged in alternating layers along the c-axis to effectively accommodate the size difference[27,28], and the [AO] layer (having A of a lower ionic radius) would create oxygen vacancies to ease the lattice distortion. This is the reason that the A-site double perovskite is more often expressed as $AA'B_2O_5$ rather than $AA'B_2O_6$.

At present, two families of double perovskite oxides have been identified with high potential as cathode materials for the SOFC technology. Firstly, there is a family of $A_2BB'O_6$ compounds, mainly including Sr_2FeNbO_6[29], Sr_2NiMoO_6[30], Sr_2CoMoO_6[31,32], and Sr_2FeMoO_6 (SFM)[33-35]. Among them, SFM has become a research hotspot of ceramic cathode materials in recent years and has a cubic structure with high structural symmetry[33], in which Sr^{2+} occupies the A-site and Fe^{3+} and Mo^{3+} reside in B-sites and B'-sites, respectively. It is a promising cathode material for SOFC for the following reasons: it is an MIEC[34], its structural symmetry is conducive to electron conduction[35], it has a modest thermal expansion coefficient compatible

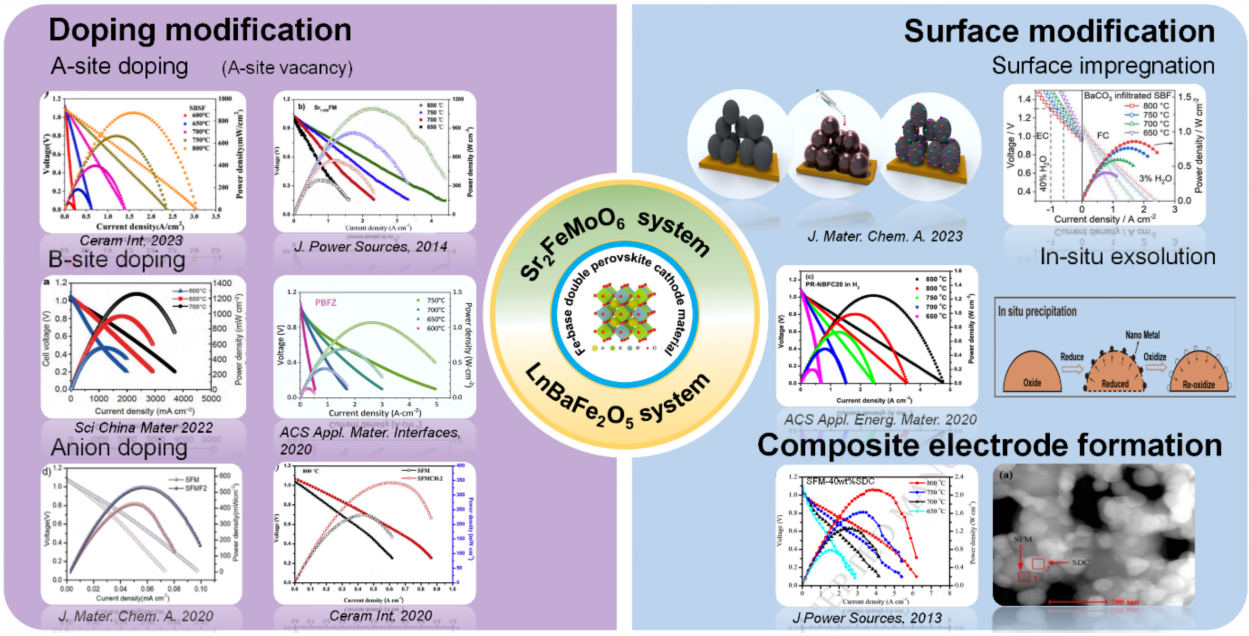

Figure 3. Summary of research activities on Fe-based double perovskite cathode.

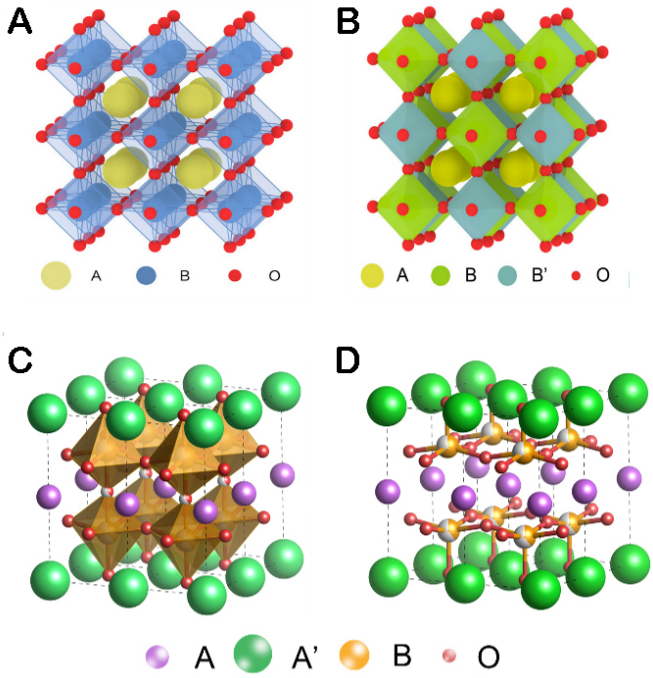

Figure 4. Structure characteristics of different perovskites: (A) Cubic crystal structure of ABO_3 perovskite (Reproduced from[5], copyright of Progress in Chemistry, 2022). (B) Cubic crystal structure of B-site double perovskite $A_2BB'O_6$ (Reproduced from[5], copyright of Progress in Chemistry, 2022). (C) Cubic crystal structure of A-site double perovskite $AA'B_2O_6$. (D) Tetragonal crystal structure of A-site double perovskite $AA'B_2O_5$.

with typical electrolytes, and it has remarkable structure stability. Another group of identified cathode materials belongs to the $AA'B_2O_5$ family, including $LnBaMn_2O_5$[36], $LnBaFe_2O_5$[37-39], and $LnBaCo_2O_5$[40], where Ln refers to Lanthanide elements. For example, some members of $LnBaFe_2O_5$ have a layered structure in which Fe occupies the B-site and Ln and Ba are located in the A- and A'-sites, respectively. Apparently, this structure supports high catalytic activity due to excellent oxygen diffusion within the structure and dynamic

oxygen exchange on the surface[37,38]. It also possesses a thermal expansion coefficient more comparable with the common medium-temperature electrolytes such as $Sm_{0.2}Ce_{0.8}O_{1.9}$ (SDC) and $La_{0.9}Sr_{0.1}Ga_{0.8}Mg_{0.2}O_{3-\delta}$ (LSGM)[38-40]. However, they still suffer from insufficient conductivity and catalytic activity[41,42] to be an effective cathode material in commercial IT-SOFC technology.

This review will focus on the progress made of SFM and $LnBaFe_2O_5$ (Ln = La, Pr, Nd, Sm, Gd), with a particular focus on the approaches employed to enhance their DC conductivity and ORR catalytic activity as a cathode material in SOFC. As seen, there are three main approaches; one is through various doping modifications, including A-site doping, B-site doping, and anion doping (replacing O^{2-})[43-45], and another is on surface modifications such as surface impregnation and *in-situ* exsolution[46-48], and finally through forming composite cathodes. The bulk of this review centers on the progress made of SFM and $LnBaFe_2O_5$ in relation to these approaches.

To enable rational comparisons between different published works, the DC conductivity data, area specific resistance (ASR) data, and peak power density (PPD) data are all quoted typically at 700-800 °C where possible. In addition, the context for discussing the coefficient of thermal expansion (CTE) of the cathode material is on its compatibility with a common electrolyte used in the SOFC technology. This includes SDC (CTE = 12.8×10^{-6} K^{-1}), LSGM (CTE = 12.2×10^{-6} K^{-1})[49], and yttrium stabilized zirconia (YSZ, CTE = 10.8×10^{-6} K^{-1})[50].

Sr_2FeMoO_6 (SFM) system

Double perovskite SFM originates from simple perovskite $SrFeO_3$. $SrFeO_3$ has limited ORR activity due to a high degree of oxygen ordering[51], which limits the concentration and mobility of oxygen vacancies[52,53]. To overcome this limitation, Mo-doping in Fe-site was proposed and investigated. Since Mo exists in high valence states of Mo^{5+} and Mo^{6+}[54] when doped in $SrFeO_3$, it increases both the electron conduction and oxygen vacancy formation of the doped SFM, making it an important cathode candidate today.

It has been shown that in an oxidizing atmosphere, $SrFe_{1-x}Mo_xO_3$ retains as a simple perovskite oxide of cubic structures regardless of the doping level of Mo[54-56]. However, in a reducing atmosphere, it is possible to make double perovskite $SrFe_{1-x}Mo_xO_3$ at high Mo-doping levels of x = 0.25-0.60, with the B-site being occupied orderly by Fe and Mo[54-58]. It has also been realized that the preparation of a pure phase $SrFe_{1-x}Mo_xO_3$ in air is also not as straightforward as anticipated. While in the past, it has been shown that by adjusting the Fe/Mo ratio, a pure $SrFe_{1-x}Mo_xO_3$ phase could be synthesized, it has, however, limited to the cases where Fe is in minor proportions[59-61]. This is due to the susceptibility of Fe and Mo ions to selective oxidation in an oxidizing atmosphere, leading to the formation of the by-product phase of $SrMoO_4$ and/or $SrMoO_3$[62].

A breakthrough emerged in 2010 when Liu *et al.* pioneered the synthesis of a pure phase double perovskite $Sr_2Fe_{1.5}Mo_{0.5}O_6$ ($SFM_{0.5}$) in air[63]. Soon after, $SFM_{0.5}$ was recognized as an ideal cathode candidate for the SOFC technology due to its excellent conductivity and oxygen catalytic performance. Extensive effort has since been made by the research community to further improve its electrochemical performance as a cathode material for SOFC. The following is our attempt to provide a summary of the recent progress of this material.

Pure phase $Sr_2Fe_{1.5}Mo_{0.5}O_6$ ($SFM_{0.5}$)

As mentioned, Liu *et al.* successfully synthesized the pure phase $SFM_{0.5}$ in the air by a microwave-assisted combustion method[63]. The success stems from the realization that excessive Fe and Mo are selectively

oxidized in the air during synthesis; this prompted them to employ a Fe-rich chemical precursor in the synthesis. The resulting $SFM_{0.5}$ possesses a desired double perovskite cubic structure, achieves a DC conductivity of 250 S·cm^{-1} and an ASR of 0.66 Ω·cm^2 at 750 °C in air and delivers a PPD of 0.340 W·cm^{-2} at 750 °C. Further studies have also shown that $SFM_{0.5}$ exhibits excellent ORR activity not only in oxygen but also in hydrogen/hydrocarbon/alcohol fuels. For example, the $SFM_{0.5}$ | LSGM | $SFM_{0.5}$ single cell achieved peak power densities of 0.500, 0.230, and 0.391 W·cm^{-2} in wet H_2[64], CH_4[65], and CH_3OH[66] fuels, respectively, at 800 °C. It also demonstrated high resistance to carbon deposition and sulphur poisoning.

Doping modification of $SFM_{0.5}$

To understand the doping effect in $SFM_{0.5}$, it is important to remember that SFM is a B-site double perovskite, where Sr^{2+} sits at A-site and Fe^{3+} and Mo^{3+} are located at B- and B'-sites, respectively.

(1) A-site doping

Among published studies on A-site doping in $SFM_{0.5}$, the doping elements may be classified into two groups. One group contains elements with the same valence state as Sr^{2+} but of different ionic radius, and the other consists of elements with different valence states from Sr^{2+}.

For example, alkaline earth metal elements, such as Ca and Ba, have been reported as A-site dopants in $SFM_{0.5}$[67-70]. They both have the same valence state as Sr^{2+} but of different ionic radius where $r_{Ca^{2+}}(0.099\ nm) < r_{Sr^{2+}}(0.113\ nm) < r_{Ba^{2+}}(0.135\ nm)$. It is argued that when the smaller-sized Ca^{2+} partially substitutes Sr^{2+} at the A-site, it would reduce the average number of coordinating lattice oxygen and increase the vacancy oxygen. This should improve the catalytic activity of $SFM_{0.5}$ for ORR. Indeed, Qiao *et al.* showed that the polarization ASR of $Sr_{1.6}Ca_{0.4}Fe_{1.5}Mo_{0.5}O_6$ ($SCa_{0.4}FM_{0.5}$) is only 0.23 Ω·cm^2 at 750 °C, ~45% lower than that of the undoped $SFM_{0.5}$ (0.42 Ω·cm^2)[67]. In addition, the conductivity of $SCa_{0.4}FM_{0.5}$ reaches 15.1 S·cm^{-1} at 750 °C, twice times higher than $SFM_{0.5}$ (7.5 S·cm^{-1}). The CTE of $SCa_{0.4}FM_{0.5}$ is also found to reduce to 15.4 × 10^{-6} K^{-1} (from 16.3 × 10^{-6} K^{-1} of $SFM_{0.5}$), making it even more comparable to electrolytes. On the other hand, doping of larger-sized Ba^{2+} at A-sites is also considered beneficial. It is argued that it would not only stabilize the cubic structure of $SFM_{0.5}$ based on the Goldschmidt tolerance factor theory[69] but also increase the unit cell dimensions. Both outcomes are seen as beneficial to oxygen ion transport in the cathode. Dai *et al.* introduced Ba^{2+} in A-sites to form $Sr_{1.8}Ba_{0.2}Fe_{1.5}Mo_{0.5}O_6$ ($SBa_{0.2}FM_{0.5}$)[70]. They showed that this material retains the cubic structure, although the unit cell is significantly enlarged. As a cathode, $SBa_{0.2}FM_{0.5}$ exhibits a lower ASR of 0.19 Ω·cm^2 at 750 °C (~55% lower than 0.42 Ω·cm^2 of $SFM_{0.5}$) and a higher conductivity of 20.1 S·cm^{-1} at 750 °C (~45% higher than 11.1 Scm^{-1} of $SFM_{0.5}$).

In a very different approach, Lanthanide (Ln) rare-earth elements were also reported as the A-site dopant in $SFM_{0.5}$. Ln usually has a valence state of +3; when partially replacing Sr^{2+}, it inevitably leads to the conversion of Mo^{6+} to Mo^{5+} and Fe^{4+} to Fe^{3+}. This would decrease the DC conductivity of $SFM_{0.5}$[71,72]. For example, Qi *et al.* introduced La^{3+} in A-sites to form $La_{0.5}Sr_{1.5}Fe_{1.5}Mo_{0.5}O_6$ ($La_{0.5}SFM_{0.5}$)[72]. They showed that as a cathode, $La_{0.5}SFM_{0.5}$ exhibits a lower ASR of 0.16 Ω·cm^2 at 800 °C (~56% lower than 0.36 Ω·cm^2 of $SFM_{0.5}$) and a higher conductivity of 2.6 Scm^{-1} at 800 °C (~72% lower than 10.2 Scm^{-1} of $SFM_{0.5}$). It is also known that La-O bonds (799 ± 4 kJ·mol^{-1}) have a higher strength than Sr-O bonds (425.5 ± 16.7 kJ·mol^{-1}). Doping of La in SMF0.5 is also expected to lower its CTE. Indeed, the average CTE of $La_{0.5}SFM_{0.5}$ is 15.0 × 10^{-6} K^{-1}, which is lower than 17.1 × 10^{-6} K^{-1} of $SFM_{0.5}$ and makes it better compatible with common electrolyte materials such as SDC, YSZ, and LSGM.

Finally, A-site absence modification has also been applied to $SFM_{0.5}$ with the aim of improving ORR activity[73,74]. It is argued that partial absence of Sr^{2+} in $SFM_{0.5}$ would not only increase the oxygen vacancies but also elevate Fe^{3+} and Mo^{5+} concentrations, shifting the equilibrium of $Fe^{3+} + Mo^{5+} \leftrightarrow Mo^{6+} + Fe^{2+}$ to the right. Both will enhance the DC conductivity and ORR activity of $SFM_{0.5}$. For example, Zhen *et al.* investigated the effect of Sr-absence in $Sr_{1.95}Fe_{1.4}Co_{0.1}Mo_{0.5}O_6$ ($S_{1.95}FC_{0.1}M_{0.5}$) cathode[73]. They found that Sr absence increases the conductivity of $S_{1.95}FC_{0.1}M_{0.5}$ to 22.5 S·cm^{-1} at 750 °C (~29% higher than 17.5 S·cm^{-1} of $SFC_{0.1}M_{0.5}$, noticeably reducing its ASR to 0.15 Ω·cm^2 (~21% lower than 0.19 Ω·cm^2 of $SFC_{0.1}M_{0.5}$).

(2) B-site doping

Among the published studies on B-site doping in $SFM_{0.5}$, they may also be divided into two groups. One group consists of dopants with varied valence states, typically the transition metal elements such as Ni[75-77], Cu[78], Co[79-81], and Sn[82]. These dopants can directly influence the $Fe^{3+} + Mo^{5+} \leftrightarrow Mo^{6+} + Fe^{2+}$ equilibrium and the level of oxygen vacancies, thus influencing the DC conductivity and ORR activity of the cathode[83].

For example, Dai *et al.* used Ni^{2+} (0.072 nm) to partially substitute Fe (Fe^{2+} 0.076 nm, Fe^{3+} 0.064 nm) at B-sites to form $Sr_2Fe_{1.5-x}Ni_xMo_{0.5}O_6$ (x = 0.1, 0.2, 0.4) ($SFN_xM_{0.5}$)[75]. The selection of Ni^{2+} takes into consideration similar ionic radii between Ni^{2+} (0.072 nm) and Fe^{2+} (0.076 nm)/Fe^{3+} (0.064 nm) to maintain the structure stability of $SFM_{0.5}$. They have shown that at low doping, the conductivity of $SFNi_{0.1}M_{0.5}$ reaches 40 S·cm^{-1}, almost quadruple that of $SFM_{0.5}$ (11.5 Scm^{-1}) at 750 °C. However, when the doping levels increase to x = 0.2 and 0.4, the conductivity of $SFN_xM_{0.5}$ decreases to below that of $SFNi_{0.1}M_{0.5}$ but remains higher than $SFM_{0.5}$. As a cathode, $SFNi_{0.1}M_{0.5}$ also demonstrates a low ASR of 0.22 Ω·cm^2 at 750 °C, ~48% lower than 0.42 Ω·cm^2 of $SFM_{0.5}$. Meanwhile, Tian *et al.* doped Cu to prepare $Sr_2Fe_{1.5-x}Cu_xMo_{0.5}O_6$ ($SFCuxM_{0.5}$, x = 0.05, 0.1, 0.2, 0.3)[78]. They have also found that at low Cu-doping of x = 0.1, the conductivity of $SFCu_{0.1}M_{0.5}$ reaches 25 S·cm^{-1} at 800 °C, more than triple that of $SFM_{0.5}$ (7 S·cm^{-1}). However, when the Cu-doping level increases to x = 0.2 and 0.3, the conductivity of $SFCuxM_{0.5}$ decreases to 22 and 8 S·cm^{-1}, respectively. $SFCu_{0.1}M_{0.5}$ also has the lowest ASR value of 0.26 Ω cm^2 at 800 °C, ~40% of 0.63 Ω cm^2 of $SFM_{0.5}$. However, Cu-doping increases the CTE, particularly at higher doping levels. For example, CTE of $SFCu_{0.1}M_{0.5}$ is 14.7 × 10^{-6} K^{-1}, while $SFCu_{0.3}M_{0.5}$ shows an increased value at 16.1 × 10^{-6} K^{-1}, both in comparison to $SFM_{0.5}$ (14.5 × 10^{-6} K^{-1}). Interestingly, Co-doping at the B-site of $SFM_{0.5}$ has resulted in a much more dramatic improvement to both the conductivity and ORR activity of $SFM_{0.5}$. Pan *et al.* synthesized $Sr_2Fe_{1.4}Co_{0.1}Mo_{0.5}O_6$ ($SFCo_{0.1}M_{0.5}$) and found that it has a significantly high DC conductivity of 63 S·cm^{-1} and a very low ASR of 0.10 Ω·cm^2 at 750 °C compared to the 22 S·cm^{-1} and 0.22 Ω·cm^2 of $SFM_{0.5}$[79]. They have attributed this to the reduced oxygen vacancy formation energy due to Co-doping in $SFM_{0.5}$. He *et al.* introduced Sn-doping to the B-site in the synthesis of $Sr_2Fe_{1.5-x}Sn_xMo_{0.5}O_6$ ($SFSn_xM_{0.5}$, x = 0.1, 0.3, 0.5)[82]. They showed that at low Sn-doping of x = 0.1, the conductivity of $SFSn_{0.1}M_{0.5}$ is 9.6 S·cm^{-1} at 800 °C, higher than 8.5 S·cm^{-1} of $SFM_{0.5}$. But with an increased Sn-doping level, the conductivity of $SFSn_xM_{0.5}$ (x = 0.3, 0.5) falls below $SFM_{0.5}$. At the same time, they have also found that the ASR of $SFSn_{0.3}M_{0.5}$ is the lowest at 0.04 Ω·cm^2 at 800 °C in air, ~ 60% lower than 0.10 Ω·cm^2 of $SFM_{0.5}$. In addition, they found that the valence states of Sn in $Sr_2Fe_{1.2}Sn_{0.3}Mo_{0.5}O_6$ are Sn^{2+} and Sn^{4+}. The presence of Sn^{4+} would shift the $Fe^{3+} + Mo^{5+} \leftrightarrow Mo^{6+} + Fe^{2+}$ equilibrium to the right, thus enhancing the conductivity. Furthermore, Sn-doping was also shown to significantly reduce the oxygen vacancy formation energy of $SFSn_{0.3}M_{0.5}$ to 0.155 eV, from 0.1569 eV of $SFM_{0.5}$. This was regarded to be responsible for the improved catalytic performance of the Sn-doped $SFM_{0.5}$.

The second group of dopants includes table valence elements such as Sc[84,85], Ga[86], and Nb[87,88]. Studies have demonstrated their influence on the conductivity and ORR activity of $SFM_{0.5}$.

Both Sc and Ga have a stable valence state of Sc^{3+} and Ga^{3+}. By Sc-doping in B-site, Sun *et al.* prepared $Sr_2Fe_{1.5-x}Sc_xMo_{0.5}O_6$ ($SFSc_xM_{0.5}$, x = 0.05, 0.1)[84]. They found that Sc-doping decreases ASR and increases DC conductivity significantly at a low doping level of x = 0.05, compared to the undoped $SFM_{0.5}$. For example, ASR at 800 °C is only 0.12 Ω·cm² for $SFSc_{0.05}M_{0.5}$ and 0.14 Ω·cm² for $SFSc_{0.1}M_{0.5}$ compared to 0.25 Ω·cm² of $SFM_{0.5}$. At the same time, the DC conductivity at 800 °C reaches 27 S·cm^{-1} for $SFSc_{0.05}M_{0.5}$ compared to 17 S·cm^{-1} for $SFM_{0.5}$, but only at 12 S·cm^{-1} for $SFSc_{0.1}M_{0.5}$. Xu *et al.* reported the doping of Ga in the synthesis of $Sr_2Fe_{1.3}Ga_{0.2}Mo_{0.5}O_6$ ($SFGa_{0.2}M_{0.5}$)[86]. They showed that Ga-doping reduces the ASR of $SFGa_{0.2}M_{0.5}$ to 0.12 Ω·cm² at 800 °C for $SFGa_{0.2}M_{0.5}$, compared to 0.25 Ω·cm² of $SFM_{0.5}$. Additionally, as a cathode, $SFGa_{0.2}M_{0.5}$ shows remarkable durability in a CO_2 atmosphere. These studies suggest that even with dopants of the same valance state as Fe^{3+}, their addition could still influence $Fe^{3+} + Mo^{5+} \leftrightarrow Mo^{6+} + Fe^{2+}$ equilibrium, thus affecting the electrochemical characteristics of the doped $SFM_{0.5}$ cathode. Gou *et al.* reported the doping of Nb in B-site in the synthesis of $Sr_2Fe_{1.4}Nb_{0.1}Mo_{0.5}O_6$ ($SFNb_{0.1}M_{0.5}$)[88]. They have shown that the conductivity of $SFNb_{0.1}M_{0.5}$ is ~30% higher than $SFM_{0.5}$ over the entire temperature of 300-800 °C. At the same time, the ASR value of $SFNb_{0.1}M_{0.5}$ is 0.10·Ω cm² at 800 °C, still lower than 0.13·Ω cm² of $SFM_{0.5}$.

(3) Anion doping

Anion doping to substitute O^{2-} has also been used to enhance electrochemical performance of $SFM_{0.5}$, including doping of F^-[89,90] and Cl^-[91]. For example, it is argued that F has a slightly higher electronegativity and lower valence electron density; its doping should weaken M-O bonding in $SFM_{0.5}$, thus increasing the activity of lattice oxygen. At the same time, the ionic radius of F^- (0.133 nm) is close to that of O^{2-} (0.140 nm); its doping should not affect the cubic structure of $SFM_{0.5}$.

Zhang *et al.* prepared $SrFe_{1.5}Mo_{0.5}O_{2.9}F_{0.1}$, while in another study, Zhang *et al.* reported the synthesis of $Sr_2Fe_{1.5}Mo_{0.5}O_{5.8}F_{0.2}$ ($SFM_{0.5}F_{0.2}$) by *F*-doping[89,90]. Both studies showed that *F*-doping effectively enhances the ORR activity of $SFM_{0.5}$. The ASR value decreases to 0.07 Ω·cm² of $SFM_{0.5}F_{0.2}$ from 0.15 Ω·cm² of $SFM_{0.5}$ at 800 °C. They have attributed this to the improved surface exchangeability of O_2 and bulk diffusion of O^{2-} in $SFM_{0.5}F_{0.2}$.

Recently, Zhang *et al.* successfully prepared $Sr_2Fe_{1.5}Mo_{0.5}O_{5.8}Cl_{0.2}$ ($SFM_{0.5}Cl_{0.2}$) by *Cl*-doping[91]. They found that despite the ionic radius of Cl^- (0.181 nm) being much greater than O^{2-}, the $SFM_{0.5}Cl_{0.2}$ retains the Fm-3m cubic structure. The study showed that while *Cl*-doping results in a reduction of conductivity, it also reduces ASR. For example, at 800 °C in air, $SFM_{0.5}Cl_{0.2}$ has a conductivity of 15.2 S·cm^{-1} (compared to 25.1 S·cm^{-1} of $SFM_{0.5}$) and an ASR of 0.11 Ω·cm² (compared to 0.14Ω·cm² of $SFM_{0.5}$). In addition, $SFM_{0.5}Cl_{0.2}$ displays high electrochemical stability in the air. They believed that *Cl*-doping weakens the Fe-O-Fe bond in $SFM_{0.5}$. This would strengthen the localization of electrons and decrease the conductivity. On the other hand, *Cl*-doping also weakens the average coulombic force between B-site ions and oxygen ions. This would enhance the activity of the lattice oxygen.

Formation of composite cathode

Combining $SFM_{0.5}$ with a second phase to form a composite cathode has also been explored, with the aim of enhancing the characteristics of the $SFM_{0.5}$ cathode. Typically, the composite cathode is formed by combining $SFM_{0.5}$ with an ionic conductor that possesses high ionic conductivity and low thermal expansion coefficient through mechanical mixing[92-99]. The main objective is to extend the total three-phase boundary (TPB) areas of the cathode to support the ORR activity. It also aims to reduce the thermal expansion coefficient of $SFM_{0.5}$ to better match the common electrolytes, such as SDC, used in the SOFC technology[100-109].

He *et al.* and Dai *et al.* investigated the $SFM_{0.5}$-SDC composite electrode by mixing $SFM_{0.5}$ with SDC[100,101]. For instance, Dai *et al.* found that the $SFM_{0.5}$-SDC40 (40 wt% of SDC) composite cathode has a polarization resistance of 0.20 Ω·cm² at 800 °C in air conditions, ~26% lower than that 0.25 Ω·cm² of $SFM_{0.5}$[101]. Supported by this composite cathode, the single cell of NiO-YSZ|SZ|$SFM_{0.5}$-SDC40 delivered a PPD of 1.770 W·cm^{-2} at 800 °C, much higher than 0.880 W·cm^{-2} delivered by the $SFM_{0.5}$ cell. Naturally, the mass ratio of the two components has a great influence on the performance of the composite cathode. On top of this, Osinkin *et al.* also demonstrated that impregnating Pr_6O_{11} on the surface of $SFM_{0.5}$-SDC10 composite cathode decreases its ASR to 0.06 Ω·cm² at 800 °C, a marked reduction from 0.23 Ω·cm² of the unimpregnated $SFM_{0.5}$-SDC10[109]. They have attributed this to the increase in the number of active sites on the electrode surface.

$Sr_2Fe_{1.5}Mo_{0.5}O_6$ system performance summary

Table 1 summarizes the published data on the crystal structure, DC conductivity (σ), area specific resistance (ASR), CTE, and PPD of $SFM_{0.5}$ cathode materials at the IT range of 700-800 °C, sourced from SCI publications in the recent decade.

To facilitate a clearer understanding of the progress trend, these data are also plotted in Figure 5 against their respective publication years. With time, the DC conductivity of $SFM_{0.5}$ cathodes is progressively improved through the various modification approaches discussed. At the same time, the ASR of the cathode is largely maintained at below 0.5 Ω·cm², indicating reasonable ORR activity of the cathode. The CTE of the cathode hovers around 15.0 × 10^{-6} K^{-1} at a similar level to that of unmodified $SFM_{0.5}$. However, the PPD seems to reach its limitation of ~1.300 W·cm^{-2} and appears to polarize in two levels of either ~0.550 W·cm^{-2} or ~1.200 W·cm^{-2}.

$LnBaFe_2O_5$ (Ln = La, Pr, Nd, Sm, Gd) system

As mentioned in the introduction, $LnBaFe_2O_5$ is an A-site double perovskite, where Fe^{3+} sits at B-sites while Ln^{3+} and Ba^{2+} are located at A- and A'- sites, respectively. $LnBaFe_2O_5$ (Ln = La, Pr, Nd, Sm, Gd) are among those studied as a cathode material for SOFC. Furthermore, much of the relevant research on $LnBaFe_2O_5$ involves experimentations with various element-doping at different sites of $LnBaFe_2O_5$ with the aim of improving its electrochemical performance as a cathode.

Characteristics of $LnBaFe_2O_5$ materials

Lanthanide contraction is well known and refers to the steady decrease in radius of Ln^{3+} ions with increasing atomic number following La > Pr > Nd > Sm > Gd, where $r_{La^{3+}}$ = 0.106 nm and $r_{Gd^{3+}}$ = 0.940 nm. This contraction directly influences the crystal structure of $LnBaFe_2O_5$, dictated by the need to accommodate the radius differences between Ln^{3+} and Ba^{2+} ($r_{Ba^{2+}}$ = 0.135 nm).

For $LaBaFe_2O_5$, the moderate radius difference between La^{3+} and Ba^{3+} permits the formation of cubic crystal structures of high symmetry. As shown in Figure 4C, $LaBaFe_2O_5$ has a cubic lattice consisting of periodical arrangements of O-octahedrons inside which Fe resides. On the other end, the progressively increased size difference between Ln^{3+} and Ba^{3+} due to lanthanide contraction prevents SBF and $GdBaFe_2O_5$ (GBF) from forming cubic structures; instead, they have a less symmetrical tetragonal crystal structure, where atoms are arranged in an ordered layer structure, as depicted in Figure 4D. For $PrBaFe_2O_5$ (PBF) and $NdBaFe_2O_5$, they could be formed into cubic phases[110-114] or tetragonal phases[110,115-117], depending on variations in the synthesis methods.

Table 1. Summary of published results on the crystal structure, DC conductivity (σ), area specific resistance (ASR), coefficient of thermal expansion (CTE), and peak power density (PPD) of $Sr_2Fe_{1.5}Mo_{0.5}O_6$ ($SFM_{0.5}$) cathode materials in the recent decade

Modification mode	Cathode material	Space group	σ (at given T) S·cm^{-1}	ASR (at given T) (Ω·cm^2)	CTE (× 10^{-6} K^{-1})	PPD (at given T) (W·cm^{-2})	Ref.
No modification	$Sr_2Fe_{1.5}Mo_{0.5}O_6$	Pm-3m	250.0 (750 °C)	0.14 (750 °C)	-	0.340 (750 °C)	[63]
	$Sr_2Fe_{1.5}Mo_{0.5}O_6$	Pm-3m	-	-	-	0.500 (800 °C)	[64]
A-site doping	$Sr_{1.6}Ca_{0.4}Fe_{1.5}Mo_{0.5}O_6$	Fm-3m	13.2 (800 °C)	0.14 (800 °C)	15.1	1.260 (800 °C)	[67]
	$Sr_{1.75}Ca_{0.25}Fe_{1.5}Mo_{0.5}O_6$	Pm-3m	55.7 (800 °C)	0.09 (800 °C)	-	0.709 (800 °C)	[68]
	$Sr_{1.8}Ba_{0.2}Fe_{1.5}Mo_{0.5}O_6$	Fm-3m	20.1 (750 °C)	0.19 (750 °C)	15.7	1.300 (750 °C)	[70]
	$La_{0.5}Sr_{1.5}Fe_{1.5}Mo_{0.5}O_6$	Fm-3m	23.0 (800 °C)	0.16 (800 °C)	15.0	1.156 (800 °C)	[72]
	$Sr_{1.95}Fe_{1.4}Co_{0.1}Mo_{0.5}O_6$	Pm-3m	22.5 (750 °C)	0.15 (750 °C)	-	-	[73]
	$Sr_{1.95}Fe_{1.5}Mo_{0.5}O_6$	Pm-3m	25.0 (800 °C)	0.16 (800 °C)	14.5	1.083 (800 °C)	[74]
	$K_{0.25}Sr_{1.75}Fe_{1.5}Mo_{0.5}O_6$	Pm-3m	-	-	-	0.430 (700 °C)	[43]
	$Bi_{0.1}Sr_{1.9}Fe_{1.5}Mo_{0.5}O_6$	Pm-3m	12.6 (850 °C)	0.40 (850 °C)	-	-	[20]
B-site doping	$Sr_2Fe_{1.4}Ni_{0.1}Mo_{0.5}O_6$	Pm-3m	40.0 (750 °C)	0.22 (750 °C)	16.7	1.210 (750 °C)	[75]
	$Sr_{1.95}Fe_{1.4}Ni_{0.1}Mo_{0.5}O_6$	Pm-3m	17.0 (800 °C)	0.10 (800 °C)	-	0.500 (800 °C)	[76]
	$Sr_2Fe_{1.3}Ni_{0.2}Mo_{0.5}O_6$	Fm-3m	13.5 (800 °C)	0.78 (800 °C)	-	-	[77]
	$Sr_2Fe_{1.4}Cu_{0.1}Mo_{0.5}O_6$	Fm-3m	25.0 (800 °C)	0.26 (800 °C)	14.7	-	[78]
	$Sr_2Fe_{1.0}Co_{0.5}Mo_{0.5}O_6$	Fm-3m	65.0 (750 °C)	0.06 (750 °C)	18.5	-	[79]
	$Sr_2Fe_{1.0}Co_{0.5}Mo_{0.5}O_6$	Fm-3m	-	-	-	0.046 (800 °C 0.05% H_2S/N_2)	[80]
	$Sr_2Fe_{0.4}Co_{0.8}Mo_{0.8}O_6$	Pm-3m	43.0 (600 °C)	-	-	-	[81]

	$Sr_2Fe_{1.5}Sn_{0.3}Mo_{0.2}O_6$	Fm-3m	7.2 (800 °C)	0.04 (800 °C)	16.1	0.618 (800 °C)	[82]
	$Sr_2Fe_{1.4}Mn_{0.1}Mo_{0.5}O_6$	Fm-3m	20.0 (800 °C)	1.12 (800 °C)	-	-	[83]
	$Sr_2Fe_{1.45}Sc_{0.05}Mo_{0.5}O_6$	Pm-3m	27.0 (800 °C)	0.12 (800 °C)	15.5	1.230 (800 °C)	[84]
	$Sr_{1.95}Fe_{1.4}Sc_{0.25}Mo_{0.25}O_6$	Pm-3m	-	0.04 (700 °C)	-	1.258 (700 °C)	[85]
	$Sr_2Fe_{1.3}Ga_{0.2}Mo_{0.5}O_6$	Fm-3m	-	0.12 (800 °C)	-	0.634 (800 °C)	[86]
	$Sr_2Fe_{1.4}Nb_{0.1}Mo_{0.5}O_6$	Pm-3m	20.3 (800 °C)	0.07 (800 °C)	16.1	1.102 (800 °C)	[87]
	$Sr_2Fe_{1.4}Nb_{0.1}Mo_{0.5}O_6$	Fm-3m	27.6 (600 °C)	0.10 (800 °C)	-	0.531 (800 °C)	[88]
Anion doping	$Sr_2Fe_{1.5}Mo_{0.5}O_{5.8}F_{0.2}$	Fm-3m	-	0.07 (800 °C)	-	0.534 (800 °C)	[90]
	$Sr_2Fe_{1.5}Mo_{0.5}O_{5.8}Cl_{0.2}$	Fm-3m	15.2 (800 °C)	0.11 (800 °C)	-	0.253 (800 °C)	[91]
Forming composite	$Sr_2Fe_{1.5}Mo_{0.5}O_6$-GDC (50 wt%)	Fm-3m	-	0.23 (800 °C)	-	-	[92]
	$Sr_2Fe_{1.5}Mo_{0.5}O_6$-(SDC+Na_2CO_3) (70 wt%)	Fm-3m	4.0 (750 °C)	-	-	0.360 (750 °C)_	[94]
	$Sr_2Fe_{1.5}Mo_{0.5}O_6$-BZCY (60 wt%)	Fm-3m	-	0.09 (800 °C)	-	0.396 (800 °C)	[95]
	$Sr_2Fe_{1.5}Mo_{0.5}O_6$-$CaCO_3$(10 wt%)	Fm-3m	-	0.29 (800 °C)	-	-	[96]
	$Sr_2Fe_{1.5}Mo_{0.5}O_6$-GDC(30 wt%)	Fm-3m	-	0.53 (750 °C)	-	0.191 (750 °C)	[97]
	$Sr_2Fe_{1.5}Mo_{0.5}O_6$-$(Sc_2O_3)_{0.10}(CeO_2)_{0.01}(ZrO_2)_{0.89}$ (30 wt%)	Fm-3m	-	0.13 (850 °C)	-	-	[98]
	$Sr_2Fe_{1.5}Mo_{0.5}O_6$-GDC(20 wt%)	Fm-3m	-	0.04 (800 °C)	11.0	-	[99]
	$Sr_2Fe_{1.5}Mo_{0.5}O_6$-SDC(30 wt%)	Fm-3m	1.4 (700 °C)	0.45 (700 °C)	-	0.279 (700 °C)	[100]
	$Sr_2Fe_{1.5}Mo_{0.5}O_6$-SDC(40 wt%)	Fm-3m	-	0.11 (800 °C)	13.6	1.770 (800 °C)	[101]
	$Sr_2Fe_{1.5}Mo_{0.5}O_6$-SDC(22 wt%)	Pm-3m	26.0 (750 °C)	-	-	-	[102]
	$Sr_2Fe_{1.5}Mo_{0.5}O_6$-SDC(40 wt%)	Fm-3m	-	0.26 (800 °C)	-	-	[103]

$Sr_2Fe_{1.5}Mo_{0.5}O_6$-SDC(40 wt%)	Fm-3m	-	0.48 (850 °C)	-	-	[104]
$Sr_2Fe_{1.5}Mo_{0.5}O_6$-SDC(10 wt%)	Fm-3m	-	0.15 (800 °C)	-	-	[105]
$Sr_2Fe_{1.5}Mo_{0.5}O_6$-SDC(40 wt%)	Fm-3m	-	1.41 (800 °C)	-	-	[106]
$Sr_2Fe_{1.5}Mo_{0.5}O_6$-SDC(60 wt%)	Fm-3m	-	0.21 (800 °C)	-	-	[107]
$Sr_2Fe_{1.5}Mo_{0.5}O_6$-SDC(40 wt%)	Fm-3m	-	0.32 (700 °C)	-	0.216 (700 °C)	[108]
SFM-YSZ(9.53wt%)	Fm-3m	100.0 (750 °C)	0.15 (750 °C)	-	0.265 (750 °C)	[50]
$Sr_2Fe_{1.5}Mo_{0.5}O_6$-SDC(40 wt%)	Fm-3m	-	0.41 (800 °C)	-	-	[18]

SDC: $Sm_{0.2}Ce_{0.8}O_{1.9}$; GDC: $Gd_{0.1}Ce_{0.9}O_2$; BZCY: $BaZr_{0.1}Ce_{0.8}Y_{0.1}O_3$.

From an electron conduction point of view, linear O-Fe-O bonds (i.e., bonding angle of 180°) in cubic $LaBaFe_2O_5$ are most conducive to electron conduction and are largely attributed to the relatively high DC conductivity observed in $LaBaFe_2O_5$[118,119]. In tetragonal $LnBaFe_2O_5$, however, the O-Fe-O bonds are no longer linear. In fact, the steady decrease in Ln^{3+} radius due to Lanthanide contraction leads to increasingly linear deviation of O-Fe-O bonds (progressively smaller bond angles), resulting in poorer electron conduction of $LnBaFe_2O_5$. However, the formation of orderly layered tetragonal structures creates favorable conduction pathways for oxygen vacancies. This is generally accepted to enhance the ORR activity of these compounds[120,121].

$LnBaFe_2O_5$ attracts research attention because its CTE falls within the range of 19.4×10^{-6} K^{-1} of $LaBaFe_2O_5$ to 14.6×10^{-6} K^{-1} of $YBaFe_2O_5$[110], which matches reasonably to the CTE of common electrolytes used in SOFC, as discussed in Section Types of perovskite oxide-based cathode materials. However, depending on the specific Ln element, the $LnBaFe_2O_5$ compound may display a rather different combination of DC conductivity and ORR catalytic activity; both together dictate the electrochemical performance of each cathode. Chen *et al.* reported an extensive study of $LnBaFe_2O_5$ (Ln = La, Pr, Nd, Sm, Gd) and found that the experimentally measured conductivity of $LnBaFe_2O_5$ largely follows La > Pr > Nd > Sm > Gd[110]. For example, the conductivity of $LaBaFe_2O_5$ reaches above 100 $S{\cdot}cm^{-1}$ at 700 °C, whilst that of GBF is only ~7.5 $S{\cdot}cm^{-1}$ at 700 °C. However, as indicated by the measured ASR values, they have shown that the ORR catalytic activity of $LnBaFe_2O_5$ follows Sm > Gd > Nd > Pr > La.

Doping modification in $LnBaFe_2O_5$

To appreciate the doping design, it is important to consider the following. Firstly, the A-site doping design for $LnBaFe_2O_5$ mostly employs the strategy to reduce the radius difference between the two A-sites (A and A') to achieve the desired outcome of improving DC conductivity and/or reducing ASR associated with oxygen transport. This is because the radius difference between Ln^{3+} (A-site) and Ba^{3+} (A'-site) dictates the crystal structure of $LnBaFe_2O_5$. For cubic

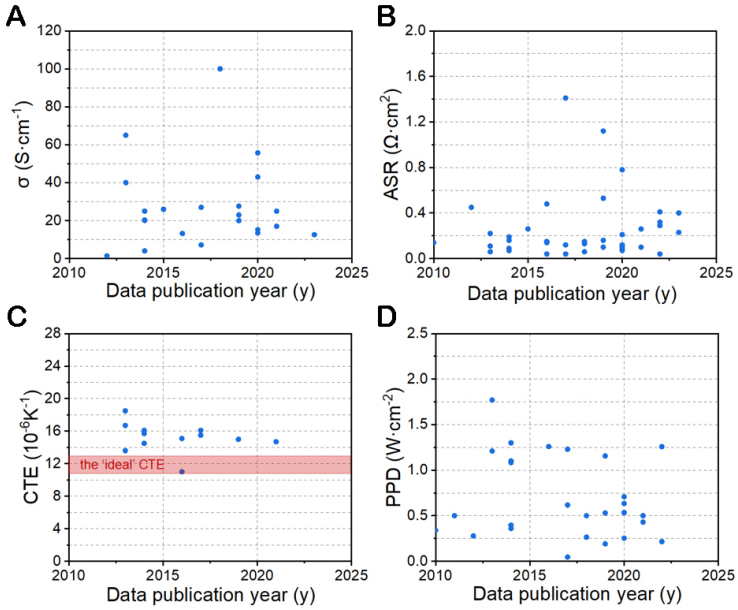

Figure 5. Plots of conductivity (A), area specific polarization resistance (ASR) (B), coefficient of thermal expansion (CTE) (C), and peak power density (PPD) (D) data of $Sr_2Fe_{1.5}Mo_{0.5}O_6$-based materials taken from Table 1 against the data publication years.

$LaBaFe_2O_5$, while the moderate radius difference between La^{3+} and Ba^{2+} permits this high symmetry structure, resulting in high DC conductivity, a reduction in the radius difference is expected to further improve structure symmetry, which is argued to benefit both electron and oxygen conduction[122]. For $LnBaFe_2O_5$ with the ordered layer structure, while the lattice supports high ORR activity due to enhanced oxygen vacancy transportation, it exhibits low DC conductivity due to the non-linear O-Fe-O bond angle impeding electron transfer. The larger the radius difference between A-site (Ln^{3+}) and A'-site (Ba^{3+}) is, the more non-linear deviation of O-Fe-O bond results, the lower the DC conductivity would be[123,124]. The B-site doping, on the other hand, is mostly directed at influencing the Fe^{3+}/Fe^{4+} transition in $LnBaFe_2O_5$ to dictate its electron conduction. This is done by introducing into B-sites either a doping element with varied valence states such as a transition metal or an element of a lower valence state than Fe^{3+}. Both aim to shift the Fe^{3+}/Fe^{4+} balance to favor the electron conduction and formation of oxygen vacancies in $LnBaFe_2O_5$[125,126].

(1) A-site doping

Here, A-site doping refers to doping in either A-sites or A'-sites of $LnBaFe_2O_5$. In this session, the following are discussed, including A'-site doping in cubic $LaBaFe_2O_5$ and doping in layer-structured $LnBaFe_2O_5$ such as A-site La^{3+}-doping in SBF, A'-site Ca^{2+}-doing in GBF, and A'-site Ba^{3+} vacancies in PBF.

Cubic $LaBaFe_2O_6$ (LBF) has a high electrical conductivity but poor ORR catalytic activity. In response, various A-site doping strategies have been studied to reduce the size difference between the two A-sites. For example, Li *et al.* synthesized $LaBa_{0.5}Sr_{0.5}Fe_2O_6$ ($LBSr_{0.5}F$) by Sr^{2+}-doping in A'-sites[122]. Sr^{2+} (1.13 Å) is smaller than Ba^{2+}, and its substitution for Ba^{2+} reduces the size difference between the two A-site ions. This would stabilize and further improve the symmetry of the cubic crystal structure of LBF. Indeed, they found that the conductivity of $LBSr_{0.5}F$ increases to 111.2 $S\cdot cm^{-1}$ at 750 °C compared to 100 $S\cdot cm^{-1}$ of the undoped LBF. More significantly, the ASR value of $LBSr_{0.5}F$ decreases to 0.15 $\Omega\cdot cm^2$ from 0.45 $\Omega\cdot cm^2$ of undoped SBF. He *et al.* used larger La^{3+} to partially substitute Sm^{2+} to reduce the size difference between the two A-sites of

SBF[123]. They have found that $Sm_{0.5}La_{0.5}BaFe_2O_5$ ($SLa_{0.5}BF$) reaches a conductivity of 31.9 S·cm^{-1} at 750 °C, which is ~3 times higher than that of the undoped SBF. At the same time, however, La^{3+}-doping was found to massively increase the ASR value to 6.15 Ω·cm^2 of $SLa_{0.5}BF$ at 750 °C, from 0.22 Ω·cm^2 of SBF. In a different approach, Wang *et al.* used the smaller Ca^{2+} to partially substitute Ba^{2+} to reduce the size difference between A-sites and A'-sites of GBF[124]. They have found that among $GdBa_{1-x}Ca_xFe_2O_5$ ($GBCa_xF$, x = 0.1, 0.2, 0.3), GBCa0.1F has a conductivity of 9.4 S·cm^{-1} at 800 °C (compared to 8.6 S·cm^{-1} of GBF), an ASR of 0.075 Ω·cm^2 at 800 °C (~60% lower than 0.10 Ω·cm^2 of GBF), and a CTE of 8.9 × 10^{-6} K^{-1} (100-900 °C). In addition, they have also observed that $GBCa_{0.2}F$ has a noticeably lower conductivity of 6.8 S·cm^{-1} at 800 °C, which was attributed to "destroyed" Ba-O bonds at high Ca substitution. Interestingly, the ASR of $GBCa_{0.2}F$ is only 0.04 Ω·cm^2 at 800 °C.

PBF has been a hot research topic as a cathode candidate for SOFC. While it has a relatively high conductivity, it has sluggish oxygen-ion transport kinetics. Recently, Chen *et al.* conducted a study on the effect of Ba vacancies (A'-site vacancies) with the aim of improving their oxygen-ion transport in PBF[127]. They have found that while $PrBa_{0.97}Fe_2O_5$ ($PBa_{0.97}F$) has just over 10% reduction in ASR (0.12 Ω·cm^2 compared to 0.14 Ω·cm^2 of PBF) at 700 °C, it also suffers ~8% reduction in conductivity relative to PBF. They have attributed this to the disruption of Ba-O bonding due to Ba deficiency. While this may result in the formation of additional oxygen vacancies benefiting ORR, as indicated by the reduction in ASR, it would also increase the likelihood of electrons being captured by oxygen vacancies, thus reducing the conductivity.

(2) B-site doping

Among the published works on B-site doping in $LnBaFe_2O_5$, the dopants are often transition metal elements with radii close to Fe^{3+} or Fe^{4+}, such as Mn[113], Co[42,119,128], and Ni[129]. They can fully enter the $LnBaFe_2O_5$ lattice and directly alter the valence state of Fe.

For instance, Mao *et al.* studied Mn-doped $NdBaFe_{2-x}Mn_xO_5$ ($NBFMn_x$, x = 0.1, 0.2, 0.3)[113]. They found that at the low Mn-doping level of x = 0.1, the conductivity of NBFMn0.1 is 90 S·cm^{-1} at 700 °C, higher than 62 S·cm^{-1} of the undoped NBF. However, when Mn-doping is greater than x = 0.1, the conductivity of $NBFMn_x$ drops below that of NBF. It is believed that while Mn-doping also leads to the formation of Mn^{4+}-O^{2-}-Mn^{3+} transition path that contributes to the electron conduction, not all Mn-O bonds support this conduction. Meanwhile, Guo *et al.* conducted a study on $SmBaFe_{2-x}Co_xO_5$ ($SBFCo_x$, x = 0.5, 1.0, 1.5)[128]. They found that the conductivity of $SBFCo_{1.0}$ is 58.68 S·cm^{-1} at 850 °C, more than five times higher than that of SBF. At the same time, the ASR of $SBFCo_{1.0}$ is 0.76 Ω·cm^2 at 800 °C, lower than 1.19 Ω·cm^2 of SBF. Ivanova *et al.* investigated the Ni^{2+}-doped $PrBaFe_{2-x}Ni_xO_5$ ($PBFNi_x$, x = 0.2, 0.4, 0.6, 0.8)[129]. They show that $PBFNi_{0.2}$ retains the cubic structure as PBF, but $PBFNi_x$ changes to a tetragonal structure when x > 0.2. They have shown that this change in crystal structures lowers the activation energy for electron conduction, thereby significantly enhancing the conductivity. For example, the conductivity of PBFNi0.8 reaches 120 S·cm^{-1} at 800 °C, much higher than 60 S·cm^{-1} of PBF.

In addition to the transitional metals, other B-site dopants, including the stable valence elements such as Sc[130], Nb[114,131], and Zn[132], have also been shown to improve the conductivity and ORR activity of $LnBaFe_2O_5$.

For example, by the Sc-doping in the B-sites, He *et al.* studied $PrBaFe_{1.6}Sc_{0.4}O_5$ ($PBFSc_{0.4}$)[130]. While they found that Sc-doping significantly reduces the conductivity, it also reduces the ASR remarkably. At 800 °C,

the conductivity of $PBFSc_{0.4}$ is measured at 5.7 S·cm^{-1}, ~77% lower than PBF, whilst the ASR is 0.05 Ω·cm^2, ~64% lower than PBF). For instance, Li *et al.* studied Nb^{5+}-doped $LaBaFe_{2-x}Nb_xO_6$ ($LBFNb_x$, x = 0.050, 0.075, 0.100)[131]. They showed that Nb^{5+}-doping enhances the ORR activity of the cathode at 800 °C (ASR = 0.06 Ω·cm^2 for $LBFNb_{0.075}$, compared to ASR = 0.16 Ω·cm^2 of LBF). This is attributed to reduced activation energy of ORR (Ea = 0.95~0.98 eV for $LBFNb_{0.075}$, compared to 1.05 eV for LBF). On the other hand, they have also reported the conductivity of $LBFNb_{0.075}$ is 50 S·cm^{-1} at 800 °C, lower than LBF. Interestingly, a study by Mao *et al.* reported the conductivity of NdBFNb0.1 reaches 81.0 S·cm^{-1} at 700 °C, more than 20% higher than NBF[114]. Clearly, more work needs to be carried out to fully understand the impact of Nb^{5+}-doping. Ren *et al.* studied Zn-doped $PrBaFe_{2-x}Zn_xO_5$ ($PBFZn_x$, x = 0.05, 0.10, 0.15, 0.20) with the aim of enhancing the oxygen catalytic capacity[132]. They found that PBFZn0.10 not only reaches a maximum conductivity of 34 S·cm^{-1} at 750 °C (twice of 17 S·cm^{-1} of the undoped PBF), it also exhibits an ASR as low as 0.06 Ω·cm^2 at 750 °C, ~73% lower than PBF (0.23 Ω·cm^2). Meanwhile, there are also reports on the study of high valence Nb^{5+}-doping in $LnBaFe_2O_5$.

Electrode surface modification of $LnBaFe_2O_5$

To enhance the oxygen catalytic activity of $LnBaFe_2O_5$, surface modification methods, such as surface impregnation and *in-situ* precipitation, were experimented with and reported for $LnBaFe_2O_5$[17,133-136].

For example, Li *et al.* investigated the surface coating of SDC nanoparticles on Ni^{2+}-doped $GdBaFeNiO_5$ (GBFNi1.0) cathodes by repeated impregnation[133]. The resulting SDC@GBFNi1.0 was found to exhibit a remarkably decreased ASR of 0.07 Ω·cm^2 at 700 °C from 0.92 Ω·cm^2 without the modification. This was attributed to the effective creation of intimate interfaces between the cathode and SDC electrolyte and the extension of the three-phase interface on the cathode to support the ORR process.

In addition, *in-situ* precipitation of nano metallic particles on the cathode surface has also been shown to increase the catalytic activity of the cathode[134,135]. Recently, in their study of Co-doped $NdBaFe_{2-x}Co_xO_5$ ($NBFCo_x$, x = 0.1,0.2), Jiang *et al.* observed the *in-situ* precipitation of $Co_{0.72}Fe_{0.28}$ nanoparticles when $NBFCo_x$ was reduced at 850 °C in 5%H_2-Ar atmosphere[136]. This *in-situ* surface modification was attributed to the significantly increased power density of the cathode. The peak power densities of the reduced $NBFCo_{0.1}$ and $NBFCo_{0.2}$ single cells are found to be 0.860 and 0.987 W·cm^{-2} at 800 °C in wet H_2, respectively, significantly higher than 0.642 W·cm^{-2} of NBF.

$LnBaFe_2O_5$ (Ln = La, Pr, Nd, Sm, Gd) performance summary

Table 2 summarizes the published data on the crystal structure, DC conductivity (σ), ASR, CTE, and PPD of $LnBaFe_2O_5$-based cathode materials at the IT range of 700-800 °C, sourced from SCI publications in the recent decade.

Figure 6 plots these reported data against the years of publication. The DC conductivity of this cathode system seems to peak at below 120 S·cm^{-1}, and PBF and $LaBaFe_2O_5$ cathodes tend to have higher conductivity. However, the ASR is reduced noticeably with time and is largely maintained at below 0.2 Ω·cm^2, indicating high ORR activity of the cathode. This is particularly notable for $LaBaFe_2O_5$; its ASR is reduced from 0.95 to 0.09 Ω·cm^2 within this time period. The PPD of this cathode system improved significantly in this time period, with PBF pushing over 1.200 W·cm^{-2}. The CTE of the cathode hovers around 16.0 × 10^{-6} K^{-1}, still higher than most of the common electrolytes.

It is worth noting that PBF-based cathodes seem to stand out for this system. Unlike $LaBaFe_2O_5$, which mostly forms into cubic structures, PBF has the ability to form into both cubic and tetragonal layered

Table 2. Summary of published data on the crystal structure, DC conductivity (σ), area specific resistance (ASR), coefficient of thermal expansion (CTE), and peak power density (PPD) of $LnBaFe_2O_5$-based cathode materials in the recent decade

Modification mode	Cathode material	Space group	σ (at given T) ($S \cdot cm^{-1}$)	ASR (at given T) ($\Omega \cdot cm^2$)	CTE ($\times 10^{-6}$ K^{-1})	PPD (at given T) ($W \cdot cm^{-2}$)	Ref.
No modification	$LaBaFe_2O_5$	Pm-3m	100.0 (700 °C)	0.95 (700 °C)	19.4	0.265 (700 °C)	[110]
	$PrBaFe_2O_5$	Pm-3m	31.5 (700 °C)	0.62 (700 °C)	18.7	0.283 (700 °C)	[110]
	$NdBaFe_2O_5$	Pmmm	15.1 (700 °C)	0.36 (700 °C)	18.3	0.308 (700 °C)	[110]
	$SmBaFe_2O_5$	Pmmm	7.5 (700 °C)	0.15 (700 °C)	16.1	0.462 (700 °C)	[110]
	$GdBaFe_2O_5$	Pmmm	1.2 (700 °C)	0.25 (700 °C)	15.6	0.396 (700 °C)	[110]
A-site doping	$SmBa_{0.5}Sr_{0.5}Fe_2O_5$	P4/mmm	22.0 (800 °C)	0.02 (800 °C)	16.2	0.874 (800 °C)	[45]
	$PrBa_{0.5}Sr_{0.5}Fe_2O_5$	Pm-3m	40.3 (800 °C)	0.03 (800 °C)	14.7	0.791 (800 °C)	[111]
	$LaBa_{0.5}Sr_{0.5}Fe_2O_6$	Pm-3m	111.2 (750 °C)	0.15 (750 °C)	18.2	0.370 (750 °C)	[122]
	$Sm_{0.8}La_{0.2}BaFe_2O_5$	Pmmm	17.5 (750 °C)	0.24 (750 °C)	16.5	0.377 (750 °C)	[123]
	$GdBa_{0.8}Ca_{0.2}Fe_2O_5$	Pmmm	6.8 (800 °C)	0.04 (800 °C)	9.1	-	[124]
	$PrBa_{0.97}Fe_2O_5$	Pmmm	22.3 (700 °C)	0.12 (700 °C)	15.2	0.183 (700 °C)	[127]
	$Pr_{0.93}BaFe_2O_5$	Pmmm	4.3 (600 °C)	0.13 (700 °C)	15.9	0.967 (700 °C)	[118]
B-site doping	$PrBaFe_{1.9}W_{0.1}O_5$	P4/mmm	52.5 (800 °C)	0.03 (800 °C)	14.6	1.020 (800 °C)	[19]
	$PrBaCo_{0.5}Fe_{1.5}O_5$	Pmmm	11.1 (700 °C)	0.14 (700 °C)	19.1	-	[38]
	$LaBa_{0.5}Sr_{0.5}Fe_2O_{5.875-d}F_{0.125}$	Pm-3m	75.6 (750 °C)	0.09 (750 °C)	18.0	0.511 (750 °C)	[39]
	$GdBaFeCoO_5$	Pmmm	450 (700 °C)	0.07 (650 °C)	16.6	0.280 (700 °C)	[42]
	$PrBaFe_{1.8}Ta_{0.2}O_5$	Pm-3m	18.2 (800 °C)	0.17 (800 °C)	12.9	0.234 (800 °C)	[112]
	$NdBaFe_{1.9}Mn_{0.1}O_5$	Pm-3m	90.0 (700 °C)	0.06 (700°C)	-	0.453 (700 °C)	[113]
	$NdBaFe_{1.9}Nb_{0.1}O_5$	Pm-3m	91.0 (700 °C)	0.14 (700°C)	-	0.392 (700 °C)	[114]
	$PrBaFe_{1.9}Mo_{0.1}O_5$	P4/mmm	17.4 (800 °C)	0.09 (800 °C)	14.5	0.680 (800 °C)	[115]
	$PrBaFe_{1.9}Ga_{0.1}O_5$	P4/mmm	54.2 (750 °C)	0.08 (750 °C)	-	0.856 (750 °C)	[116]
	$PrBaFe_{1.9}Zr_{0.1}O_5$	P4/mmm	-	0.13 (700 °C)	-	1.260 (700 °C)	[117]
	$PrBaFe_{1.8}Co_{0.2}O_5$	Pmmm	53.9 (800 °C)	0.03 (800 °C)	-	0.735 (850 °C)	[119]
	$PrBaFe_{1.9}Sn_{0.1}O_5$	P4/mmm	-	0.14 (800 °C)	-	0.709 (800 °C)	[125]
	$LaBaFe_{1.85}Sn_{0.15}O_5$	Pm-3m	16.0 (800°C)	0.07 (800 °C)	17.7	0.514 (800 °C)	[126]
	$PrBaFe_{1.9}Ni_{0.1}O_5$	P4/mmm	120.0 (800°C)	-	21.6	-	[129]
	$PrBaFe_{1.6}Sc_{0.4}O_5$	P4/mmm	5.7 (800 °C)	0.05 (800 °C)	-	0.921 (850 °C)	[130]
	$LaBaFe_{1.925}Nb_{0.075}O_6$	Pm-3m	50.0 (800 °C)	0.06 (800 °C)	18.6	0.553 (800 °C)	[131]
	$PrBaFe_{1.9}Zn_{0.1}O_5$	P4/mmm	34.0 (750 °C)	0.06 (750 °C)	16.4	1.060 (750 °C)	[132]
Surface modification	$BaCO_3$@$SmBaFe_2O_5$	P4/mmm	16.2 (700 °C)	0.07 (700 °C)	-	0.593 (700 °C)	[17]
	SDC@$GdBaFe_2O_5$	Pmmm	4.2 (700 °C)	0.07 (700°C)	17.0	0.350 (700 °C)	[133]
	$Co_{0.72}Fe_{0.28}$@$LnBaFe_2O_5$	Pm-3m	10.8 (850 °C)	0.38 (850 °C)	17.4	0.987 (800 °C)	[136]

structures. Sitting at this transition position seems to give PBF the advantage of both structures; thus, it seems to have both high conductivity and high ORR activity.

SUMMARY AND PROSPECT

In the last decades, much research has been conducted on Fe-based double perovskite materials, leading to significant advances in their performance as the cathode material in SOFC technology. This paper presents an overview of the research progress on two types of Fe-based double perovskite cathodes, namely SFM and $LnBaFe_2O_5$ (Ln = La, Pr, Nd, Sm, Gd). It is focused on the impact of modification approaches, including element-doping, surface modification, and forming composite cathodes on the electrochemical characteristics (DC conductivity, ORR activity as indicated by the ASR and PPD), and CTE (in the context of compatibility to common electrolytes used in SOFC technology).

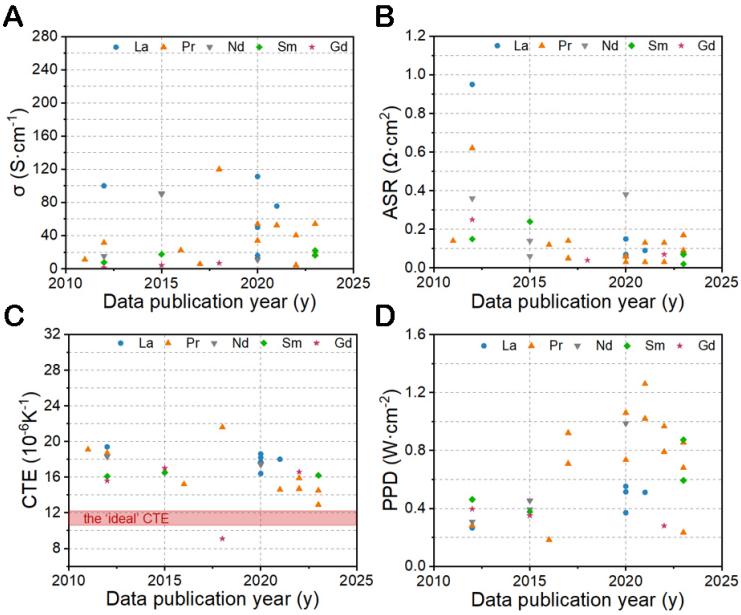

Figure 6. Plots of conductivity (A), area specific polarization resistance (ASR) (B), coefficient of thermal expansion (CTE) (C), and peak power density (PPD) (D) data of $LnBaFe_2O_5$-based materials taken from Table 2 against the data publication years.

This focused review examines the impact of various doping elements, including alkaline earth metals (Sr, Ca, Ba), transition metals (Fe, Co, Ni, Sc), and other elements (Zn, Nd, Y), in relationship to different doping modes, including A-site doping, B-site doping, and anion doping, to the two cathode systems. The review attempts to provide clear scientific rationales for different doping designs in order to support the understanding of a large volume of reported empirical data. This review has shown that elemental doping in Fe-based double perovskite can influence the conductivity and catalytic activity of the material concurrently but not necessarily in the same desired direction. For example, doping of La^{3+} in $SmBaFe_2O_{5+\delta}$ has been shown to increase the conductivity but reduce the catalytic activity; on the contrary, doping of Nb^{5+} in LBF results in decreased conductivity but increased catalytic activity. Depending on the relative influences of the two, the impact of doping on the electrochemical performance of the cathode could be either positive or negative. When trying to negotiate the doping effect on the thermal expansion coefficient and the electrochemical properties, there is again an added level of complexity. For example, Sr-doping improves the conductivity of $LaBaFe_2O_5$ but fails to resolve its high thermal expansion coefficient; on the contrary, doping with Ca or Sc reduces the thermal expansion coefficient as desired but also reduces the conductivity. So far, When the doped elements are Co^{3+}, Sn^{2+}, and F^-, $SFM_{0.5}$ cathodes show the best performance of conductivity and oxygen catalytic activity. For $LnBaFe_2O_5$ cathodes, Mn^{3+}-doped $NdBaFe_2O_5$ and Zn^{2+}-doped PBF have the best performance.

It seems that to optimize the overall electrochemical performance of the Fe-based double perovskite cathode, it is necessary to determine an optimal doping ratio through both A- and B-site modification. To achieve rational doping design, we must put effort into a mechanistic understanding of the impact of doping element(s) on the perovskite structure, oxygen and/or metal defects, and chemical stability of these materials, on top of the collecting empirical cathode performance data. This will enable us to balance the doping impact of all key properties, such as conductivity, catalytic activity, structure and chemical stability, and thermal expansion, in order to achieve the required electrochemical performance as a cathode. From the various pieces of experimental evidence reported so far, there remains further potential to enhance the Fe-based double perovskite cathodes for advanced SOFC technology.

While surface modification and the creation of composite cathodes can also be used to further improve the performance of these cathode materials, the effect of such approaches is, however, limited to mostly an incremental improvement of the base material it concerns.

DECLARATIONS

Authors' contributions

Data sourcing, collection, and analysis, draft and revision of manuscript: Xie M, Cai C
Data sourcing: Duan X, Xue K
Overall supervising, design and review of the manuscript, providing funding: An S
Supervising data analysis, review, revision, and editing of the manuscript: Yang H

Availability of data and materials

Data will be made available upon request.

Financial support and sponsorship

The project was supported by the National Natural Science Foundation of China (51974167), the Natural Science Foundation Youth Foundation of Inner Mongolia (2023QN05038), and the higher education carbon peak carbon neutral research project Inner Mongolia Autonomous Region (STZX202210).

Conflicts of interest

All authors declare that there are no conflicts of interest.

Ethical approval and consent to participate

Not applicable.

Consent for publication

Not applicable.

Author's Note

While we fully recognize that it is the convention to denote a perovskite oxide, for example, $O_{3-\delta}$ in $La_{1-x}Sr_xMnO_{3-\delta}$ to indicate the general presence of oxygen vacancies in these compounds, for the simplicity and easy visualization, we have adopted the formula as $La_{1-x}Sr_xMnO_3$ (drop off δ) in this article. This will apply to all perovskite oxide systems discussed in this paper.

REFERENCES

1. Chen Y, Sun H, Guo J, et al. Research on carbon-based and metal-based negative electrode materials via DFT calculation for high potassium storage performance: a review. *Energy Mater* 2023;3:300045. DOI
2. Bianchi F, Bosio B, Conte F, et al. Modelling and optimal management of renewable energy communities using reversible solid oxide cells. *Appl Energy* 2023;334:120657. DOI
3. Zhu B, Mi Y, Xia C, et al. A nanoscale perspective on solid oxide and semiconductor membrane fuel cells: materials and technology. *Energy Mater* 2022;1:100002. DOI
4. van Biert L, Godjevac M, Visser K, Aravind P. A review of fuel cell systems for maritime applications. *J Power Sources* 2016;327:345-64. DOI
5. Zhang Y, Zhang M, Zhao H. Double perovskite material as anode for solid oxide fuel cells. *Prog Chem* 2022;34:272-84. DOI
6. Abdalla AM, Hossain S, Azad AT, et al. Nanomaterials for solid oxide fuel cells: a review. *Renew Sustain Energ Rev* 2018;82:353-68. DOI
7. Shu L, Sunarso J, Hashim SS, Mao J, Zhou W, Liang F. Advanced perovskite anodes for solid oxide fuel cells: a review. *Int J Hydrog Energy* 2019;44:31275-304. DOI

8. Singh M, Zappa D, Comini E. Solid oxide fuel cell: decade of progress, future perspectives and challenges. *Int J Hydrog Energy* 2021;46:27643-74. DOI
9. Wang J, Liu M, Lin M. Oxygen reduction reactions in the SOFC cathode of Ag/CeO_2. *Solid State Ion* 2006;177:939-47. DOI
10. Horita T, Yamaji K, Sakai N, et al. Imaging of oxygen transport at SOFC cathode/electrolyte interfaces by a novel technique. *J Power Sources* 2002;106:224-30. DOI
11. Radhakrishnan R, Virkar AV, Singhal SC. Estimation of charge-transfer resistivity of Pt Cathode on YSZ Electrolyte Using Patterned Electrodes. *J Electrochem Soc* 2005;152:A927. DOI
12. Lee SY, Yun J, Tai W. Synthesis of Ni-doped $LaSrMnO_3$ nanopowders by hydrothermal method for SOFC interconnect applications. *Adv Powder Technol* 2018;29:2423-8. DOI
13. Cai C, Xie M, Xue K, et al. Enhanced electrochemical performance of $La_{0.6}Sr_{0.4}Co_{0.2}Fe_{0.8}O_{3-\delta}$ cathode via Ba-doping for intermediate-temperature solid oxide fuel cells. *Nano Res* 2022;15:3264-72. DOI
14. Xie M, Cai C, Liu X, et al. Improved durability of high-performance intermediate-temperature solid oxide fuel cells with a Ba-doped $La_{0.6}Sr_{0.4}Co_{0.2}Fe_{0.8}O_{3-\delta}$ cathode. *ACS Appl Mater Interfaces* 2022;14:33052-63. DOI
15. Guo D, Li A, Lu C, Qiu D, Niu B, Wang B. High activity and stability of cobalt-free $SmBa_{0.5}Sr_{0.5}Fe_2O_{5+\delta}$ perovskite oxide as cathode material for solid oxide fuel cells. *Ceram Int* 2023;49:34277-90. DOI
16. Carneiro JSA, Brocca RA, Lucena MLRS, Nikolla E. Optimizing cathode materials for intermediate-temperature solid oxide fuel cells (SOFCs): oxygen reduction on nanostructured lanthanum nickelate oxides. *Appl Catal B Environ* 2017;200:106-13. DOI
17. Zhang M, Du Z, Sun Z, Zhao H. Unraveling the promotional role of $BaCO_3$ in the electrode reaction kinetics of an $SmBaFe_2O_{5+\delta}$ air electrode of reversible solid oxide cells. *J Mater Chem A* 2023;11:21645-54. DOI
18. Wang Y, Liu T. A highly active and stable $Sr_2Fe_{1.5}Mo_{0.5}O_{6-\delta}$-$Ce_{0.8}Sm_{0.2}O_{1.95}$ ceramic fuel electrode for efficient hydrogen production via a steam electrolyzer without safe gas. *Int J Coal Sci Technol* 2022;9:4. DOI
19. Zhang B, Wan Y, Hua Z, Tang K, Xia C. Tungsten-doped $PrBaFe_2O_{5+\delta}$ double perovskite as a high-performance electrode material for symmetrical solid oxide fuel cells. *ACS Appl Energy Mater* 2021;4:8401-9. DOI
20. Yang M, Yao Z, Liu S, et al. Bismuth doped $Sr_2Fe_{1.5}Mo_{0.5}O_{6-\delta}$ double perovskite as a robust fuel electrode in ceramic oxide cells for direct CO_2 electrolysis. *J Mater Sci Technol* 2023;164:160-7. DOI
21. Zhu Z, Sun K, Xu D, et al. Enhancing the performance of symmetrical solid oxide fuel cells with $Sr_2Fe_{1.5}Mo_{0.5}O_{6-\delta}$ electrodes via infiltration of Pr_6O_{11} bifunctional catalyst. *Electrochim Acta* 2022;402:139569. DOI
22. Zhang W, Zhang Z, Guo L, Ma T. Double perovskite material as an electrode for intermediate-temperature solid oxide fuel cells application. *Prog Chem* 2016;28:961-74. Avaliable from: https://manu56.magtech.com.cn/progchem/EN/abstract/abstract11656.shtml [Last accessed on 6 Feb 2024].
23. Hussain S, Li Y. Review of solid oxide fuel cell materials: cathode, anode, and electrolyte. *Energy Transit* 2020;4:113-26. DOI
24. Afroze S, Karim A, Cheok Q, Eriksson S, Azad AK. Latest development of double perovskite electrode materials for solid oxide fuel cells: a review. *Front Energy* 2019;13:770-97. DOI
25. Ishihara T. Perovskite oxide for solid oxide fuel cells. New York: Springer; 2009. pp. 1-16.
26. Anderson M, Greenwood K, Taylor G, Poeppelmeier K. B-cation arrangements in double perovskites. *Prog Solid State Chem* 1993;22:197-233. DOI
27. King G, Woodward PM. Cation ordering in perovskites. *J Mater Chem* 2010;20:5785-96. DOI
28. Zheng K, Świerczek K, Bratek J, Klimkowicz A. Cation-ordered perovskite-type anode and cathode materials for solid oxide fuel cells. *Solid State Ion* 2014;262:354-8. DOI
29. Rosas J, Cervantes J, León-flores J, et al. DFT study on the electronic and magnetic properties of the Sr_2FeNbO_6 compound. *Mater Today Commun* 2020;23:100844. DOI
30. Skutina L, Filonova E, Medvedev D, Maignan A. Undoped Sr_2MMoO_6 double perovskite molybdates (M = Ni, Mg, Fe) as promising anode materials for solid oxide fuel cells. *Materials* 2021;14:1715. DOI PubMed PMC
31. Kumar P, Jena P, Patro PK, et al. Influence of lanthanum doping on structural and electrical/electrochemical properties of double perovskite Sr_2CoMoO_6 as anode materials for intermediate-temperature solid oxide fuel cells. *ACS Appl Mater Interfaces* 2019;11:24659-67. DOI
32. Zhang P, Huang Y, Cheng J, Mao Z, Goodenough JB. Sr_2CoMoO_6 anode for solid oxide fuel cell running on H_2 and CH_4 fuels. *J Power Sources* 2011;196:1738-43. DOI
33. Zheng K, Lach J, Zhao H, Huang X, Qi K. Magnesium-doped $Sr_2(Fe,Mo)O_{6-\delta}$ double perovskites with excellent redox stability as stable electrode materials for symmetrical solid oxide fuel cells. *Membranes* 2022;12:1006. DOI PubMed PMC
34. Qiu P, Sun S, Li J, Jia L. A review on the application of $Sr_2Fe_{1.5}Mo_{0.5}O_6$-based oxides in solid oxide electrochemical cells. *Sep Purif Technol* 2022;298:121581. DOI
35. Liu Q, Yang C, Dong X, Chen F. Perovskite $Sr_2Fe_{1.5}Mo_{0.5}O_{6-\delta}$ as electrode materials for symmetrical solid oxide electrolysis cells. *Int J Hydrog Energy* 2010;35:10039-44. DOI
36. Zhang Y, Zhao H, Du Z, Świerczek K, Li Y. High-performance $SmBaMn_2O_{5+\delta}$ electrode for symmetrical solid oxide fuel cell. *Chem Mater* 2019;31:3784-93. DOI
37. Ding H, Xue X. $BaZr_{0.1}Ce_{0.7}Y_{0.1}Yb_{0.1}O_{3-\delta}$ electrolyte-based solid oxide fuel cells with cobalt-free $PrBaFe_2O_{5+\delta}$ layered perovskite cathode. *J Power Sources* 2010;195:7038-41. DOI

38. Zhao L, Shen J, He B, Chen F, Xia C. Synthesis, characterization and evaluation of $PrBaCo_{2-x}FexO_{5+\delta}$ as cathodes for intermediate-temperature solid oxide fuel cells. *Int J Hydrog Energy* 2011;36:3658-65. DOI
39. Li H, Lü Z. High-performance fluorine-doped cobalt-free oxide as a potential cathode material for solid oxide fuel cells. *Int J Hydrog Energy* 2021;46:2503-10. DOI
40. Yu A, Xia T, Sun L, Li Q, Huo L, Zhao H. Effects of rare earth doping on electrochemical properties of $NdBaCo_2O_{6-\delta}$ cathode materials. *J Alloy Compd* 2020;837:155563. DOI
41. Alvarado-flores JJ, Mondragón-sánchez R, Ávalos-rodríguez ML, Alcaraz-vera JV, Rutiaga-quiñones JG, Guevara-martínez SJ. Synthesis, characterization and kinetic study of the $Sr_2FeMoO_{6-\delta}$ double perovskite: new findings on the calcination of one of its precursors. *Int J Hydrog Energy* 2021;46:26185-96. DOI
42. Zhang Z, Li X, Xu H. A highly operating stability, oxygen reduction reaction active and CO_2/Cr tolerance perovskite cathode for solid oxide fuel cells. *J Alloy Compd* 2022;922:166119. DOI
43. Yang Y, Shi N, Xie Y, et al. K doping as a rational method to enhance the sluggish air-electrode reaction kinetics for proton-conducting solid oxide cells. *Electrochim Acta* 2021;389:138453. DOI
44. Akkurt S, Sindiraç C, Özmen Egesoy T, ERĞEN E. A review on new cobalt-free cathode materials for reversible solid oxide fuel cells. *J Met Mater Miner* 2023;33:1654. DOI
45. Gao Y, Zhang M, Fu M, Hu W, Tong H, Tao Z. A comprehensive review of recent progresses in cathode materials for proton-conducting SOFCs. *Energy Rev* 2023;2:100038. DOI
46. Rath MK, Lee K. Superior electrochemical performance of non-precious Co-Ni-Mo alloy catalyst-impregnated $Sr_2FeMoO_{6-\delta}$ as an electrode material for symmetric solid oxide fuel cells. *Electrochim Acta* 2016;212:678-85. DOI
47. Qiu P, Lin J, Lei L, et al. Evaluation of Cr-tolerance of $Sr_2Fe_{1.5}M_{o0.5}O_{6-\delta}$ cathode for solid oxide fuel cells. *ACS Appl Energy Mate* 2019;2:7619-27. DOI
48. Liu J, Lei Y, Li Y, et al. Infiltrated $Sr_2Fe_{1.5}Mo_{0.5}O_{6-\delta}/La_{0.9}Sr_{0.1}Ga_{0.8}Mg_{0.2}O_3$ electrodes towards high performance symmetrical solid oxide fuel cells fabricated by an ultra-fast and time-saving procedure. *Electrochem Commun* 2017;78:6-10. DOI
49. Han X, Chen P, Wu M, et al. A redox-reversible perovskite electrode for CeO_2-and $LaGaO_3$-based symmetric solid oxide fuel cells. *Ceram Int* 2022;48:26440-51. DOI
50. Li Y, Zou S, Ju J, Xia C. Characteristics of nano-structured SFM infiltrated onto YSZ backbone for symmetrical and reversible solid oxide cells. *Solid State Ion* 2018;319:98-104. DOI
51. Xiao G, Liu Q, Wang S, et al. Synthesis and characterization of Mo-doped $SrFeO_{3-\delta}$ as cathode materials for solid oxide fuel cells. *J Power Sources* 2012;202:63-9. DOI
52. Patrakeev M, Leonidov I, Kozhevnikov V, Kharton V. Ion-electron transport in strontium ferrites: relationships with structural features and stability. *Solid State Sci* 2004;6:907-13. DOI
53. Schmidt M, Campbell S. Crystal and magnetic structures of $Sr_2Fe_2O_5$ at elevated temperature. *J Solid State Chem* 2001;156:292-304. DOI
54. Savinskaya O, Nemudry AP. Oxygen transport properties of nanostructured $SrFe_{1-x}Mo_xO_{2.5+3/2x}$ ($0 < x < 0.1$) perovskites. *J Solid State Electrochem* 2011;15:269-75. DOI
55. Liu G, Rao G, Feng X, et al. Structural transition and atomic ordering in the non-stoichiometric double perovskite $Sr_2Fe_xMo_{2-x}O_6$. *J Alloy Compd* 2003;353:42-7. DOI
56. Zhang L, Zhou Q, He Q, He T. Double-perovskites $A_2FeMoO_{6-\delta}$ (A=Ca, Sr, Ba) as anodes for solid oxide fuel cells. *J Power Sources* 2010;195:6356-66. DOI
57. Xiao G, Liu Q, Dong X, Huang K, Chen F. $Sr_2Fe_{4/3}Mo_{2/3}O_6$ as anodes for solid oxide fuel cells. *J Power Sources* 2010;195:8071-4. DOI
58. Markov A, Leonidov I, Patrakeev M, et al. Structural stability and electrical transport in $SrFe_{1-x}Mo_xO_{3-\delta}$. *Solid State Ion* 2008;179:1050-3. DOI
59. Zhang SL, Zhang AP, Li CX, Yang GJ, Li CJ. Suspension plasma sprayed $Sr_2Fe_{1.4}Mo_{0.6}O_{6-\delta}$ electrodes for solid oxide fuel cells. *J Therm Spray Tech* 2017;26:432-40. DOI
60. Li H, Zhao Y, Wang Y, Li Y. $Sr_2Fe_{2-x}Mo_xO_{6-\delta}$ perovskite as an anode in a solid oxide fuel cell: Effect of the substitution ratio. *Catal Today* 2016;259:417-22. DOI
61. Rager J, Zipperle M, Sharma A, Macmanus-driscoll JL. Oxygen Stoichiometry in Sr_2FeMoO_6, the determination of Fe and Mo valence states, and the chemical phase diagram of SrO-Fe_3O_4-MoO_3. *J Am Ceram Soc* 2004;87:1330-5. DOI
62. Liu Q, Dong X, Xiao G, Chen F. $Sr_2Fe_{1.5}Mo_{0.5}O_{6-\delta}$ as both anode and cathode materials for symmetrical SOFCs. Proceedings of the 218th ECS Meeting; 2010 Oct 10-15; Las Vegas, USA. Pennington: Electrochemical Society; 2011.
63. Liu Q, Dong X, Xiao G, Zhao F, Chen F. A novel electrode material for symmetrical SOFCs. *Adv Mater* 2010;22:5478-82. DOI
64. Liu Q, Bugaris DE, Xiao G, et al. $Sr_2Fe_{1.5}Mo_{0.5}O_{6-\delta}$ as a regenerative anode for solid oxide fuel cells. *J Power Sources* 2011;196:9148-53. DOI
65. Zheng K, Świerczek K, Polfus JM, Sunding MF, Pishahang M, Norby T. Carbon deposition and sulfur poisoning in $SrFe_{0.75}Mo_{0.25}O_{3-\delta}$ and $SrFe_{0.5}Mn_{0.25}Mo_{0.25}O_{3-\delta}$ electrode materials for symmetrical SOFCs. *J Electrochem Soc* 2015;162:F1078-87. DOI
66. Li H, Tian Y, Wang Z, Qie F, Li Y. An all perovskite direct methanol solid oxide fuel cell with high resistance to carbon formation at the anode. *RSC Adv* 2012;2:3857-63. DOI
67. Qiao J, Chen W, Wang W, et al. The Ca element effect on the enhancement performance of $Sr_2Fe_{1.5}Mo_{0.5}O_{6-\delta}$ perovskite as cathode

for intermediate-temperature solid oxide fuel cells. *J Power Sources* 2016;331:400-7. DOI

68. Xu Z, Hu X, Wan Y, et al. Electrochemical performance and anode reaction process for Ca doped $Sr_2Fe_{1.5}Mo_{0.5}O_{6-\delta}$ as electrodes for symmetrical solid oxide fuel cells. *Electrochim Acta* 2020;341:136067. DOI
69. Goldschmidt VM. Die gesetze der krystallochemie. *Naturwissenschaften* 1926;14:477-85. DOI
70. Dai N, Wang Z, Jiang T, et al. A new family of barium-doped $Sr_2Fe_{1.5}Mo_{0.5}O_{6-\delta}$ perovskites for application in intermediate temperature solid oxide fuel cells. *J Power Sources* 2014;268:176-82. DOI
71. Forbess MJ, Seraji S, Wu Y, Nguyen CP, Cao GZ. Dielectric properties of layered perovskite $Sr_{1-x}A_xBi_2Nb_2O_9$ ferroelectrics (A=La, Ca and x=0,0.1). *Appl Phys Lett* 2000;76:2934-6. DOI
72. Qi H, Thomas T, Li W, et al. Reduced thermal expansion and enhanced redox reversibility of $La_{0.5}Sr_{1.5}Fe_{1.5}Mo_{0.5}O_{6-\delta}$ anode material for solid oxide fuel cells. *ACS Appl Energy Mater* 2019;2:4244-54. DOI
73. Zhen S, Sun W, Tang G, Rooney D, Sun K, Ma X. Evaluation of strontium-site-deficient $Sr_2Fe_{1.4}Co_{0.1}Mo_{0.5}O_{6-\delta}$-based perovskite oxides as intermediate temperature solid oxide fuel cell cathodes. *Int J Hydrog Energy* 2016;41:9538-46. DOI
74. Yang G, Feng J, Sun W, et al. The characteristic of strontium-site deficient perovskites $Sr_xFe_{1.5}Mo_{0.5}O_{6-\delta}$ (x = 1.9-2.0) as intermediate-temperature solid oxide fuel cell cathodes. *J Power Sources* 2014;268:771-7. DOI
75. Dai N, Feng J, Wang Z, et al. Synthesis and characterization of B-site Ni-doped perovskites $Sr_2Fe_{1.5-x}Ni_xMo_{0.5}O_{6-\delta}$ (x = 0, 0.05, 0.1, 0.2, 0.4) as cathodes for SOFCs. *J Mater Chem A* 2013;1:14147-53. DOI
76. Osinkin D, Antonova E, Shubin K, Bogdanovich N. Influence of nickel exsolution on the electrochemical performance and rate-determining stages of hydrogen oxidation on $Sr_{1.95}Fe_{1.4}Ni_{0.1}Mo_{0.5}O_{6-\delta}$ promising electrode for solid state electrochemical devices. *Electrochim Acta* 2021;369:137673. DOI
77. Meng X, Wang Y, Zhao Y, et al. In-situ exsolution of nanoparticles from Ni substituted $Sr_2Fe_{1.5}Mo_{0.5}O_{6-\delta}$ perovskite oxides with different Ni doping contents. *Electrochim Acta* 2020;348:136351. DOI
78. Tian C, Cheng J, Yang J. A highly active cathode material of Cu-doped $Sr_2Fe_{1.5}Mo_{0.5}O_6$ for symmetrical solid oxide fuel cells. *J Mater Sci Mater Electron* 2021;32:1258-64. DOI
79. Pan X, Wang Z, He B, Wang S, Wu X, Xia C. Effect of Co doping on the electrochemical properties of $Sr_2Fe_{1.5}Mo_{0.5}O_6$ electrode for solid oxide fuel cell. *Int J Hydrog Energy* 2013;38:4108-15. DOI
80. Song Y, Zhong Q, Wang D, Xu Y, Tan W. Interaction between electrode materials $Sr_2FeCo_{0.5}Mo_{0.5}O_{6-\delta}$ and hydrogen sulfide in symmetrical solid oxide fuel cells. *Int J Hydrog Energy* 2017;42:22266-72. DOI
81. Stanley P, Hussain AM, Huang Y, Gritton JE, Wachsman ED. Defect chemistry and oxygen non-stoichiometry in $SrFe_{0.2}Co_{0.4}Mo_{0.4}O_{3-\delta}$ ceramic oxide for solid oxide fuel cells. *Ionics* 2020;26:5641-9. DOI
82. He B, Gong C, Wang Z, Jia L, Zhao L. Novel, cobalt-free, and highly active $Sr_2Fe_{1.5}Mo_{0.5-x}Sn_xO_{6-\delta}$ cathode materials for intermediate temperature solid oxide fuel cells. *Int J Hydrog Energy* 2017;42:10308-16. DOI
83. Jiang Y, Yang Y, Xia C, Bouwmeester HJM. $Sr_2Fe_{1.4}Mn_{0.1}Mo_{0.5}O_{6-\delta}$ perovskite cathode for highly efficient CO_2 electrolysis. *J Mater Chem A* 2019;7:22939-49. DOI
84. Sun W, Li P, Xu C, et al. Investigation of Sc doped $Sr_2Fe_{1.5}Mo_{0.5}O_6$ as a cathode material for intermediate temperature solid oxide fuel cells. *J Power Sources* 2017;343:237-45. DOI
85. Zhang L, Yin Y, Xu Y, Yu S, Bi L. Tailoring $Sr_2Fe_{1.5}Mo_{0.5}O_{6-\delta}$ with Sc as a new single-phase cathode for proton-conducting solid oxide fuel cells. *Sci China Mater* 2022;65:1485-94. DOI
86. Xu C, Sun K, Yang X, et al. Highly active and CO_2-tolerant $Sr_2Fe_{1.3}Ga_{0.2}Mo_{0.5}O_{6-\delta}$ cathode for intermediate-temperature solid oxide fuel cells. *J Power Sources* 2020;450:227722. DOI
87. Hou M, Sun W, Li P, et al. Investigation into the effect of molybdenum-site substitution on the performance of $Sr_2Fe_{1.5}Mo_{0.5}O_{6-\delta}$ for intermediate temperature solid oxide fuel cells. *J Power Sources* 2014;272:759-65. DOI
88. Gou M, Ren R, Sun W, et al. Nb-doped $Sr_2Fe_{1.5}Mo_{0.5}O_{6-\delta}$ electrode with enhanced stability and electrochemical performance for symmetrical solid oxide fuel cells. *Ceram Int* 2019;45:15696-704. DOI
89. Zhang Z, Zhu Y, Zhong Y, Zhou W, Shao Z. Anion doping: a new strategy for developing high-performance perovskite-type cathode materials of solid oxide fuel cells. *Adv Energy Mater* 2017;7:1700242. DOI
90. Zhang L, Sun W, Xu C, et al. Attenuating a metal-oxygen bond of a double perovskite oxide *via* anion doping to enhance its catalytic activity for the oxygen reduction reaction. *J Mater Chem A* 2020;8:14091-8. DOI
91. Zhang Y, Zhu Z, Gu Y, Chen H, Zheng Y, Ge L. Effect of Cl doping on the electrochemical performance of $Sr_2Fe_{1.5}Mo_{0.5}O_{6-\delta}$ cathode material for solid oxide fuel cells. *Ceram Inter* 2020;46:22787-96. DOI
92. Zare A, Salari H, Babaei A, Abdoli H, Aslannejad H. Electrochemical evaluation of $Sr_2Fe_{1.5}Mo_{0.5}O_{6-\delta}/Ce_{0.9}Gd_{0.1}O_{1.95}$ cathode of SOFCs by EIS and DRT analysis. *J Electroanal Chem* 2023;936:117376. DOI
93. Xu J, Wan S, Wang Y, et al. Enhancing performance of molybdenum doped strontium ferrite electrode by surface modification through Ni infiltration. *Int J Hydrog Energy* 2021;46:10876-91. DOI
94. Dong X, Tian L, Li J, Zhao Y, Tian Y, Li Y. Single layer fuel cell based on a composite of $Ce_{0.8}Sm_{0.2}O_{2-\delta}$-$Na_2CO_3$ and a mixed ionic and electronic conductor $Sr_2Fe_{1.5}Mo_{0.5}O_{6-\delta}$. *J Power Sources* 2014;249:270-6. DOI
95. Li M, Ni M, Su F, Xia C. Proton conducting intermediate-temperature solid oxide fuel cells using new perovskite type cathodes. *J Power Sources* 2014;260:197-204. DOI
96. Zhang L, Xu C, Sun W, et al. Constructing perovskite/alkaline-earth metal composite heterostructure by infiltration to revitalize CO_2 electrolysis. *Sep Purif Technol* 2022;298:121475. DOI

97. Guo Y, Guo T, Zhou S, et al. Characterization of $Sr_2Fe_{1.5}Mo_{0.5}O_{6-\delta}$-$Gd_{0.1}Ce_{0.9}O_{1.95}$ symmetrical electrode for reversible solid oxide cells. *Ceram Int* 2019;45:10969-75. DOI
98. Maide M, Lillmaa K, Salvan LK, et al. Influence of electrolyte scaffold microstructure and loading of MIEC material on the electrochemical performance of RSOC fuel electrode. *Fuel Cells* 2018;18:789-99. DOI
99. Skafte TL, Sudireddy BR, Blennow P, Graves C. Carbon and redox tolerant infiltrated oxide fuel-electrodes for solid oxide cells. *ECS Trans* 2016;72:201-14. DOI
100. He B, Zhao L, Song S, Liu T, Chen F, Xia C. $Sr_2Fe_{1.5}Mo_{0.5}O_{6-\delta}$-$Sm_{0.2}Ce_{0.8}O_{1.9}$ composite anodes for intermediate-temperature solid oxide fuel cells. *J Electrochem Soc* 2012;159:B619-26. DOI
101. Dai N, Lou Z, Wang Z, et al. Synthesis and electrochemical characterization of $Sr_2Fe_{1.5}Mo_{0.5}O_6$-$Sm_{0.2}Ce_{0.8}O_{1.9}$ composite cathode for intermediate-temperature solid oxide fuel cells. *J Power Sources* 2013;243:766-72. DOI
102. Hu B, Wang Y, Zhu Z, Xia C, Bouwmeester HJM. Measuring oxygen surface exchange kinetics on mixed-conducting composites by electrical conductivity relaxation. *J Mater Chem A* 2015;3:10296-302. DOI
103. Wang Y, Liu T, Fang S, Xiao G, Wang H, Chen F. A novel clean and effective syngas production system based on partial oxidation of methane assisted solid oxide co-electrolysis process. *J Power Sources* 2015;277:261-7. DOI
104. Wang Y, Liu T, Fang S, Chen F. Syngas production on a symmetrical solid oxide H_2O/CO_2 co-electrolysis cell with $Sr_2Fe_{1.5}Mo_{0.5}O_6$-$Sm_{0.2}Ce_{0.8}O_{1.9}$ electrodes. *J Power Sources* 2016;305:240-8. DOI
105. Osinkin D, Lobachevskaya N, Suntsov AY. The electrochemical behavior of the promising $Sr_2Fe_{1.5}Mo_{0.5}O_{6-\delta}$+$Ce_{0.8}Sm_{0.2}O_{1.9-\delta}$ anode for the intermediate temperature solid oxide fuel cells. *J Alloy Compd* 2017;708:451-5. DOI
106. Wang Y, Liu T, Lei L, Chen F. Methane assisted solid oxide co-electrolysis process for syngas production. *J Power Sources* 2017;344:119-27. DOI
107. Farzin YA, Babaei A, Skafte TL, Stamate E, Ataie A, Jensen SH. Low-temperature preparation and investigation of electrochemical properties of SFM/CGO composite electrode. *Solid State Ion* 2020;356:115435. DOI
108. Li C, Zhang Q, Liu W, Tian X, Zheng R, Liu J. Tailoring the electrolyte and cathode properties for optimizing the performance of symmetrical solid oxide fuel cells fabricated by one-step co-sintering method. *J Asian Ceram Soc* 2022;10:386-95. DOI
109. Osinkin D, Beresnev S, Bogdanovich N. Influence of Pr_6O_{11} on oxygen electroreduction kinetics and electrochemical performance of $Sr_2Fe_{1.5}Mo_{0.5}O_{6-\delta}$ based cathode. *J Power Sources* 2018;392:41-7. DOI
110. Chen D, Wang F, Shi H, Ran R, Shao Z. Systematic evaluation of Co-free $LnBaFe_2O_{5+\delta}$ (Ln=Lanthanides or Y) oxides towards the application as cathodes for intermediate-temperature solid oxide fuel cells. *Electrochim Acta* 2012;78:466-74. DOI
111. Wen C, Chen K, Guo D, et al. High performance and stability of $PrBa_{0.5}Sr_{0.5}Fe_2O_{5+\delta}$ symmetrical electrode for intermediate temperature solid oxide fuel cells. *Solid State Ion* 2022;386:116048. DOI
112. Liu C, Wang F, Ni Y, et al. Ta-doped $PrBaFe_2O_{5+\delta}$ double perovskite as a high-performance electrode material for symmetrical solid oxide fuel cells. *Int J Hydrog Energy* 2023;48:9812-22. DOI
113. Mao X, Yu T, Ma G. Performance of cobalt-free double-perovskite $NdBaFe_{2-x}MnxO_{5+\delta}$ cathode materials for proton-conducting IT-SOFC. *J Alloy Compd* 2015;637:286-90. DOI
114. Mao X, Wang W, Ma G. A novel cobalt-free double-perovskite $NdBaFe_{1.9}Nb_{0.1}O_{5+\delta}$ cathode material for proton-conducting IT-SOFC. *Ceram Int* 2015;41:10276-80. DOI
115. Zhang H, Yang J, Wang P, Yao C, Yu X, Shi F. Novel cobalt-free perovskite $PrBaFe_{1.9}Mo_{0.1}O_{5+\delta}$ as a cathode material for solid oxide fuel cells. *Solid State Ion* 2023;391:116144. DOI
116. Zhang B, Zhang S, Han H, Tang K, Xia C. Cobalt-free double perovskite oxide as a promising cathode for solid oxide fuel cells. *ACS Appl Mater Interfaces* 2023;15:8253-62. DOI
117. Li G, Gou Y, Cheng X, et al. Enhanced electrochemical performance of the Fe-based layered perovskite oxygen electrode for reversible solid oxide cells. *ACS Appl Mater Interfaces* 2021;13:34282-91. DOI
118. Lü S, Zhu Y, Fu X, et al. A-site deficient Fe-based double perovskite oxides $Pr_xBaFe_2O_{5+\delta}$ as cathodes for solid oxide fuel cells. *J Alloy Compd* 2022;911:165002. DOI
119. Zhang K, Ge L, Ran R, Shao Z, Liu S. Synthesis, characterization and evaluation of cation-ordered $LnBaCo_2O_{5+\delta}$ as materials of oxygen permeation membranes and cathodes of SOFCs. *Acta Mater* 2008;56:4876-89. DOI
120. Lu C, Niu B, Yi W, Ji Y, Xu B. Efficient symmetrical electrodes of $PrBaFe_{2-x}Co_xO_{5+\delta}$ (x=0, 0.2,0.4) for solid oxide fuel cells and solid oxide electrolysis cells. *Electrochim Acta* 2020;358:136916. DOI
121. Chavez E, Mueller M, Mogni L, Caneiro A. Study of $LnBaCo_2O_{6-\delta}$ (Ln = Pr, Nd, Sm and Gd) double perovskites as new cathode material for IT-SOFC. *J Phys Conf Ser* 2009;167:012043. DOI
122. Li H, Lü Z. A highly stable cobalt-free $LaBa_{0.5}Sr_{0.5}Fe_2O_{6-\delta}$ oxide as a high performance cathode material for solid oxide fuel cells. *Int J Hydrog Energy* 2020;45:19831-9. DOI
123. He Z, Xia L, Chen Y, Yu J, Huang X, Yu Y. Layered perovskite $Sm_{1-x}La_xBaFe_2O_{5+\delta}$ as cobalt-free cathodes for IT-SOFCs. *RSC Adv* 2015;5:57592-8. DOI
124. Wang L, Xie P, Bian L, Liu X, Chou K. Performance of Ca-doped $GdBa_{1-x}Ca_xFe_2O_{5+\delta}$ (x = 0, 0.1) as cathode materials for IT-SOFC application. *Catal Today* 2018;318:132-6. DOI
125. Dong G, Yang C, He F, et al. Tin doped $PrBaFe_2O_{5+\delta}$ anode material for solid oxide fuel cells. *RSC Adv* 2017;7:22649-61. DOI
126. Li H, Lü Z. Highly active and stable tin-doped perovskite-type oxides as cathode materials for solid oxide fuel cells. *Electrochim Acta* 2020;361:137054. DOI

127. Chen T, Pang S, Shen X, Jiang X, Wang W. Evaluation of Ba-deficient $PrBa_{1-x}Fe_2O_{5+\delta}$ oxides as cathode materials for intermediate-temperature solid oxide fuel cells. *RSC Adv* 2016;6:13829-36. DOI
128. Guo RH, Guo L, Zhang JY, Zhou GZ, An SL. Synthesis and characterization of double perovskite cathode material $SmBaFe_{2-x}Co_xO_{5+\delta}$ for solid oxide fuel cells. *New Chem Mater* 2018;46:183-6. Avaliable from: https://webofscience.clarivate.cn/wos/alldb/full-record/CSCD:6207444 [Last accessed on 6 Feb 2024].
129. Ivanov AI, Kolotygin VA, Tsipis EV, Bredikhin SI, Kharton VV. Electrical conductivity, thermal expansion and electrochemical properties of perovskites $PrBaFe_{2-x}Ni_xO_{5+\delta}$. *Russ J Electrochem* 2018;54:533-40. DOI
130. He W, Wu X, Dong F, Ni M. A novel layered perovskite electrode for symmetrical solid oxide fuel cells: $PrBa(Fe_{0.8}Sc_{0.2})_2O_{5+\delta}$. *J Power Sources* 2017;363:16-9. DOI
131. Li H, Wei B, Su C, Wang C, Lü Z. Novel cobalt-free layered perovskite $LaBaFe_{2-x}Nb_xO_{6-\delta}$ (x = 0-0.1) as cathode for solid oxide fuel cells. *J Power Sources* 2020;453:227875. DOI
132. Ren R, Wang Z, Meng X, et al. Boosting the electrochemical performance of Fe-based layered double perovskite cathodes by Zn^{2+} doping for solid oxide fuel cells. *ACS Appl Mater Interfaces* 2020;12:23959-67. DOI
133. Li L, Jin F, Shen Y, He T. Cobalt-free double perovskite cathode $GdBaFeNiO_{5+\delta}$ and electrochemical performance improvement by $Ce_{0.8}Sm_{0.2}O_{1.9}$ impregnation for intermediate-temperature solid oxide fuel cells. *Electrochim Acta* 2015;182:682-92. DOI
134. Sengodan S, Ju Y, Kwon O, et al. Self-decorated MnO nanoparticles on double perovskite solid oxide fuel cell anode by *in situ* exsolution. *ACS Sustain Chem Eng* 2017;5:9207-13. DOI
135. Lai K, Manthiram A. Self-regenerating Co-Fe nanoparticles on perovskite oxides as a hydrocarbon fuel oxidation catalyst in solid oxide fuel cells. *Chem Mater* 2018;30:2515-25. DOI
136. Jiang J, Zhang Y, Yang X, Shen Y, He T. $NdBaFe_{2-}xCoxO_{5+\delta}$ double perovskites with exsolved Co-Fe alloy nanoparticles as highly efficient and stable anodes for direct hydrocarbon solid oxide fuel cells. *ACS Appl Energy Mater* 2021;4:134-45. DOI